# Extracellular vesicles production regulates fluconazole resistance in *Cryptococcus neoformans*

Juliana RIZZO[1,2#§], Adèle TROTTIER[1#], Frédérique MOYRAND[1#], Jean-Yves COPPEE[1#], Corinne MAUFRAIS[1,3#], Ana Claudia G. ZIMBRES[2#], Thi Tuong Vi DANG[1#], Alexandre ALANIO[8,9], Marie Desnos-OLLIVIER[8], Isabelle MOUYNA[1#], Gérard PÉHAU-ARNAUDET[4], Pierre-Henri COMMERE[5], Sophie NOVAULT[5], Iuliana V. ENE[6], Leonardo NIMRICHTER[2#], Marcio L. RODRIGUES[2,7#] and Guilhem JANBON[1,*#]

[1] Institut Pasteur, Université Paris Cité, Unité Biologie des ARN des Pathogènes Fongiques, F-75015 Paris, France
[2] Instituto de Microbiologia Paulo de Góes (IMPG), Universidade Federal do Rio de Janeiro, Rio de Janeiro, Brazil
[3] Institut Pasteur, Université Paris Cité, USR 3756 IP CNRS, HUB Bioinformatique et Biostatistique, F-75015, Paris, France
[4] Institut Pasteur, Université Paris Cité, Plateforme de Bio-Imagerie Ultrastructurale, F-75015 Paris, France
[5] Institut Pasteur, Université Paris Cité, Cytometry and Biomarkers, F-75015, Paris, France
[6] Institut Pasteur, Université Paris Cité, Fungal Heterogeneity Group, F-75015 Paris, France
[7] Instituto Carlos Chagas, Fundação Oswaldo Cruz (FIOCRUZ), Curitiba, Brazil
[8] Institut Pasteur, Université Paris Cité, Centre National de Référence Mycoses Invasives et Antifongiques, Groupe de recherche Mycologie Translationnelle, Département de Mycologie, F-75015 Paris, France
[9] Laboratoire de parasitologie-mycologie, AP-HP, Hôpital Saint-Louis, F-75010 Paris, France

* Corresponding author: janbon@pasteur.fr
[#] Members of the data sharing transparency group on fungal extracellular vesicles
§ Current affiliation: Instituto de Biofísica Carlos Chagas Filho (IBCCF), Universidade Federal do Rio de Janeiro, Rio de Janeiro, Brazil

**ABSTRACT (150/150 words)**

Resistance to fluconazole (FLC), the most widely used antifungal drug, is typically achieved by altering the azole drug target and/or drug efflux pumps. Recent reports have suggested a link between vesicular trafficking and antifungal resistance. Here, we identified novel *Cryptococcus neoformans* regulators of extracellular vesicle (EV) biogenesis that impact FLC resistance. In particular, the transcription factor Hap2 does not affect the expression of the drug target or efflux pumps, yet it impacts the cellular sterol profile. Subinhibitory FLC concentrations also downregulate EV production. Moreover, *in vitro* spontaneous FLC-resistant colonies showed altered EV production, and the acquisition of FLC resistance was associated with decreased EV production in clinical isolates. Finally, the reversion of FLC resistance was associated with increased EV production. These data suggest a model in which fungal cells can regulate EV production before regulating gene expression as a first line of defense against antifungal assault in this fungal pathogen.

## 1) INTRODUCTION

Fungal diseases have been consistently neglected despite their increasing impact on human health. These eukaryotic pathogens infect ~1.5 billion people worldwide and lead to ~1.5 million deaths annually[1,2]. Over 90% of reported fungal-associated deaths are caused by species from four genera *Aspergillus*, *Cryptococcus*, *Candida*, or *Pneumocystis*[3]. The species *Cryptococcus neoformans*, *Candida albicans*, *Candida auris,* and *Aspergillus fumigatus* form the critical priority group within the fungal pathogens list published by the World Health Organization (WHO) in 2022[4,5]. Fungal infections are generally difficult to treat, and mortality rates remain high despite available antifungal treatments[6]. The arsenal of antifungal molecules is based on four main classes: polyenes (e.g.,

50 amphotericin B), azoles (e.g., fluconazole (FLC)), echinocandins (e.g., caspofungin), and flucytosine (a
51 pyrimidine analog)[7]. Due to their bioavailability, low toxicity, and wide spectrum of action, azoles are
52 the most widely used antifungals. Azoles are fungistatic drugs that inhibit the cytochrome P450-
53 dependent enzyme 14-α demethylase encoded by *ERG11* in fungi, thus interrupting the synthesis of
54 ergosterol[6]. In azole-treated cells, an accumulation of toxic intermediate sterols is observed,
55 increasing membrane permeability and inhibiting fungal growth[8]. Prolonged use of FLC has the
56 potential to select FLC-resistant strains[8]. Azole resistance has been associated with mutations in the
57 *ERG11* sequence, thus limiting azole binding[8], or in transcription factors (TF) like *TAC1* or *UPC1*
58 regulating the expression of *ERG11* and/or drug efflux pumps[9,10]. Heteroresistance has also been
59 described in *C. neoformans*, and was associated with the unstable duplication of chromosome 1,
60 resulting in the potential overexpression of *ERG11* and the efflux pump encoding gene *AFR1*[11,12].

61 Extracellular vesicles (EVs) are cell-derived membrane particles released to the extracellular
62 space known to be produced in all domains of life. In fungi, they have been isolated from at least
63 fifteen different genera[13]. *Cryptococcus* EVs display extensive diversity in size, shape, and structure[14]
64 and most EVs appear decorated by fibrillary material composed of mannoproteins, and are covered
65 by capsule polysaccharide-like material[14]. EVs contain lipids (including ergosterol), polysaccharides,
66 small molecules, pigments, and RNAs, although our understanding of the exact composition and
67 function of these cargo molecules remains limited[12].

68 The involvement of vesicular trafficking in fungal FLC resistance has been previously
69 suggested. For instance, turbinmicin, a molecule with a broad spectrum antifungal activity, targets
70 Sec14p in the post-Golgi vesicular trafficking pathway and synergizes with FLC against *C. albicans*
71 biofilm formation[15]. Sortin2 inhibition of vesicular transport potentiates azoles in *C. albicans* and *C.*
72 *glabrata*[16]. Studies in *C. neoformans* and *S. cerevisiae* have implicated Golgi trafficking and vesicle
73 formation as potential avenues of azole potentiation[17–19]. Recent studies also suggested that EVs
74 released by fungi could play a role in antifungal resistance[20–23]. For instance, *C. albicans* EVs confer FLC
75 resistance to biofilms and ESCRT (endosomal sorting complexes required for transport) mutants
76 defective in EVs production show altered biofilm FLC resistance[20]. EVs from *C. auris* drug-resistant
77 strain induced amphotericin-B resistance to a susceptible strain[21], but the mechanisms underlying this
78 process remain largely unknown. Other examples of EVs associated with drug resistance come from
79 the study of *Leishmania* parasites[24], where EVs mediate the delivery of drug-resistance genes, leading
80 to the emergence of resistant subpopulations[24].

81 Despite these intriguing connections, the study of fungal EV biosynthesis in the context of
82 antifungal resistance has been constrained by our limited understanding of EV biosynthesis. Genetic
83 analyses of EV production and regulation have been hampered by the long and cumbersome protocols

84 necessary to isolate and study these particles. Only a handful of mutations associated with defects in
85 EV production have been reported so far, as recently reviewed[13].
86 To narrow this knowedge gap, we screened a *C. neoformans* TF mutant library[25] and identified
87 the first regulators of EV biogenesis in fungi. We present data revealing a phenotypic association
88 between drug resistance and regulation of EV biogenesis in these mutant strains but also in
89 spontaneous FLC-resistant mutants isolated *in vitro,* as well as in clinical isolates. Moreover, we
90 demonstrate that EV-defective mutants show altered lipid content. Finally, we show that sub-
91 inhibitory concentrations of FLC regulate EV production. Taken together, our study points to a new
92 mechanism of drug resistance in which cells adapt to FLC stress by modulating EV production. Our
93 results uncover key regulators of EV biogenesis in *C. neoformans*, as well as a novel link with antifungal
94 drug resistance.
95
96 **2) RESULTS**
97
98 **a) EV production is regulated by growth conditions and growth phase in *C. neoformans*.**
99 To test whether EV production varies across different media, growth stages, and
100 temperatures, we optimized a new EV isolation protocol, in which the ultracentrifugation step was
101 bypassed (**Fig 1A**). We used this protocol to demonstrate that EV production, as measured by the
102 amount of total sterol in cellular supernatants, was highest when cells were grown in synthetic
103 dextrose (SD) medium at 30°C compared to the other conditions tested (**Fig 1B**). By exploring the
104 dynamics of EV production during the growth on SD agar plates at 30°C, we noticed that cells release
105 EVs during a limited time window (16 to 24 h) corresponding to the transition between the exponential
106 to stationary growth phase (**Fig 1C**).
107

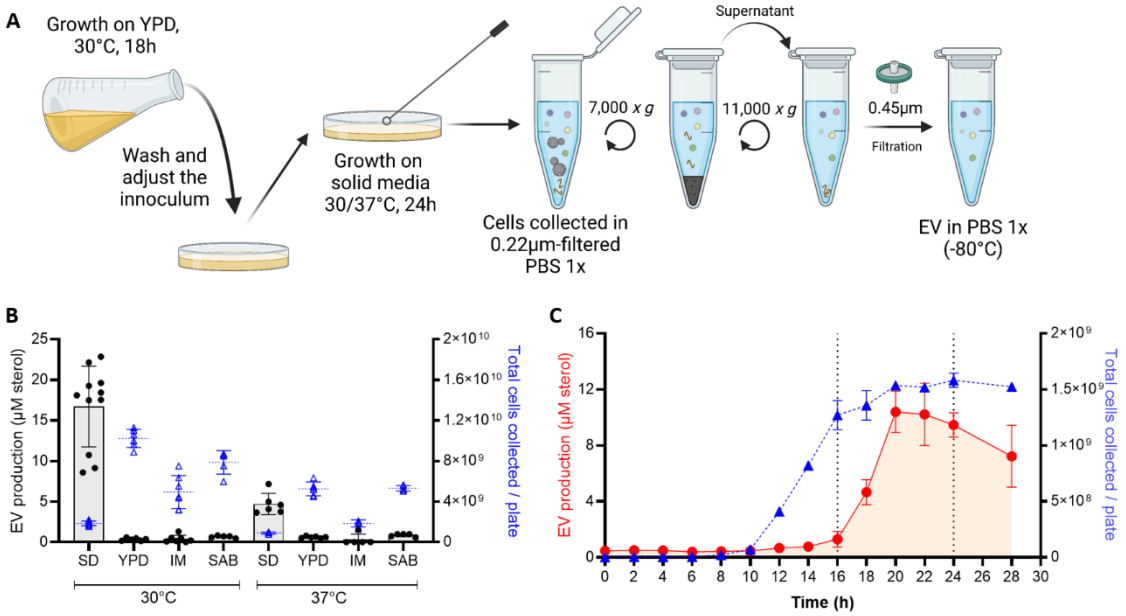


**Figure 1: EV production is regulated by growth conditions and growth phase**. Schematic representation of the optimized quick protocol used to obtain EVs from cells grown on solid medium (A). EV production from cells grown on different media: synthetic dextrose (SD), yeast extract-peptone-dextrose (YPD), capsule induction media (IM), and Sabouraud (SAB) at 30°C and 37°C, sterol concentration was normalized to the number of cells in each culture (B). EV production on SD medium at 30°C during the growth curve was analysed by the amount of total sterol in cellular supernatants when EVs are isolated using the quick protocol, values are expressed per plate of culture during each timepoint (C). Experiments were done with three or more biological replicates. Error bars show means ± SD. Schematic representation created in BioRender.

### b) Identification of regulators of EV production in *C. neoformans*.

The tight regulation between EV production and growth suggested that specific TFs might regulate their biosynthesis. Thus, to identify potential regulators of EV biogenesis, we screened a collection of 155 TF mutants[25] using the EV purification optimized protocol adjusted to 96-well plates (**Fig 2A**). We identified four mutants strongly altered in EV production. These strains produced <10% of the WT EV levels as evaluated by the total amount of sterols in EV samples. The EV-deficient strains lacked TFs *BZP2* (CNAG_04263), *GAT5* (CNAG_05153), *LIV4* (CNAG_06283) and *HAP2* (CNAG_07435). These results were confirmed when samples were prepared using the conventional untracentrifugation protocol[14], measuring the total amount of sterols **(Fig 2B),** and evaluating the number of particles by nanoparticle flow cytometry (nanoFCM) analysis **(Fig 2C).** It is important to note that despite an impressive decrease in EV levels, these TF mutants were not completely impaired in EV production, as the high sensitivity of the nanoFCM analysis used detected EV-like particles in each of the EV samples obtained from the mutants. Moreover, using a large number of culture plates, we obtained enough *hap2Δ*-derived EVs to be observed by Cryo-EM. Image analysis revealed a similar structure of *hap2Δ* EVs as previously observed for WT EVs[14] (**Fig 2D**).

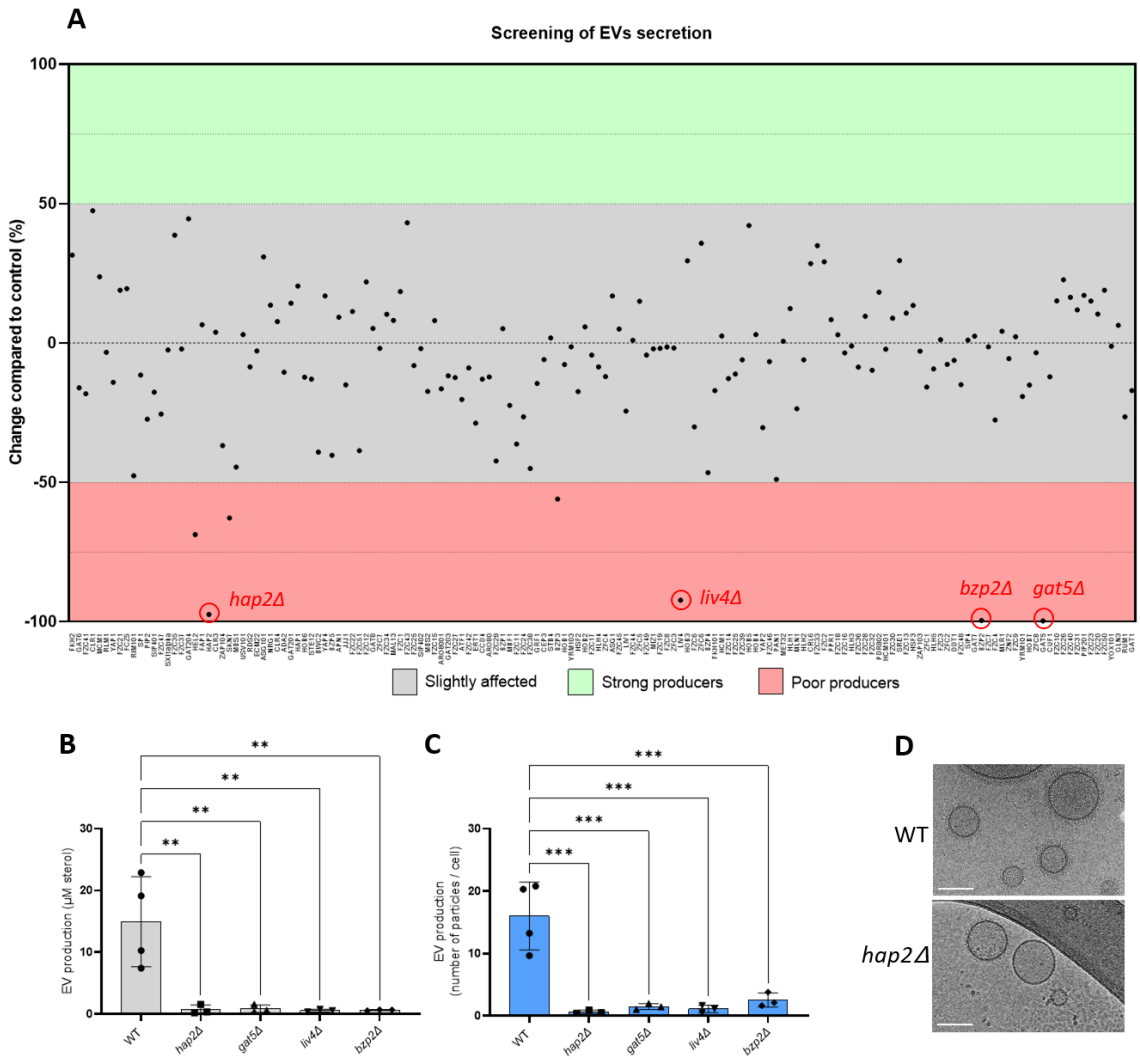


**Figure 2: Identification of the transcription factors regulating EV production in *C. neoformans***. The screening of a 155 transcription factor (TF) mutant collection identified four major EV production regulators: *HAP2*, *LIV4*, *BZP2,* and *GAT5* (A). Confirmation of the EV phenotype using independent knockout strains generated in the KN99α background by measuring the amount of total sterol contained in EV samples (B) and single particle counting using nanoFCM (C). Cryo-EM analysis of EVs obtained from WT and *hap2Δ* strains (D), scale bar = 100 nm. Sterol concentrations were normalized to the number of cells in each culture. Experiments were performed in at least three biological replicates. Error bars show means ± SD.

Bzp2p and Gat5p belong to a conserved zinc finger family containing TFs known as GATA-factors, regulating radiation sensitivity and nitrogen catabolite repression (NCR) when preferred nitrogen sources are absent or limiting[26]. Liv4p is a conserved MYB-like DNA-binding domain TF regulating growth and virulence in *C. neoformans*[27]. Hap2p is a subunit of the evolutionary conserved CCAAT-binding heme activator protein (HAP) complex, a heterotrimeric complex composed of Hap2/3/5 and the transcriptional activation subunit, HapX[28]. As expected, the *hap3Δ* and *hap5Δ* mutants were also drastically impaired for EV production. In contrast, the *hapXΔ* mutant strain produced the same quantity of EVs as the WT strain (**Fig 3A**), suggesting that the Hap2/3/5 complex controls EV production in an HapX-independent manner in *C. neoformans.* Notably, whereas *bzp2Δ*,

151 *liv4Δ,* and *gat5Δ* mutant strains displayed reduced growth (**Fig S1**), none of the *hap* mutant strains
152 showed growth deficiency under the conditions used to obtain EVs (**Fig 3B**).

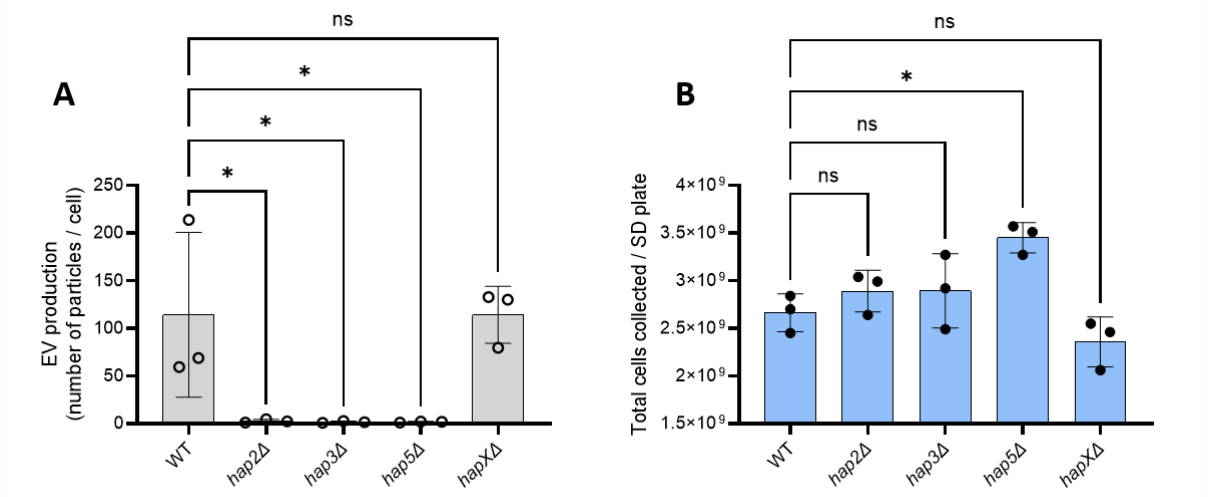


153
154 **Figure 3:** The *HAP2/3/5* complex is involved in EV secretion. Quantification of single EV particles released by WT and HAP
155 complex mutants using nanoFCM (A). Growth analysis by counting the total number of cells obtained from SD plates (B). The
156 experiments were carried out in biological triplicates. Error bars show means ± SD.

157
158 **c) Transcriptional analysis of EV-defective mutants**

159 To decipher the link between the expression of these TF and the EV production phenotype of their
160 corresponding mutants, we performed the RNA-seq analysis of the *hap2Δ*, *gat5Δ* and WT strains
161 grown for 18 h on SD plates at 30°C, a condition which corresponds to the maximum EV production
162 (see **Fig 1C**). Differential expression gene analysis identified 538 genes commonly upregulated in both
163 *hap2Δ* and *gat5Δ* strains (**Fig 4A**) (**Supplementary Table S1**). Gene ontology (GO) analysis using the
164 FungiDB database (https://fungidb.org/fungidb/app), revealed that genes associated with ribosome
165 biogenesis, transmembrane transport, and protein-containing complex assembly were enriched in this
166 set (**Fig 4B**). This suggests that the downregulation of the translation machinery expected to occur
167 during the transition from the exponential phase to the stationary phase[29] is impaired in both mutant
168 strains. On the other hand, 310 genes were downregulated in both mutant strains (**Fig 4D**)
169 (**Supplementary Table S1**). GO analysis revealed genes coding for proteins implicated in protein
170 glycosylation, signaling, carbohydrate metabolic processes, cell wall organization and biogenesis,
171 protein modification process, carbohydrate metabolism, reproductive processes, vesicle-mediated
172 transport, as well as cytokinesis, as being enriched in this set. Interestingly, *GAT5* expression is strongly
173 downregulated (10-fold) in the *hap2Δ* mutant, suggesting that Hap2 might act upstream of Gat5 in
174 regulating EV production. In contrast, neither *BZP2* nor *LIV4* appeared regulated by *HAP2* and/or
175 *GAT5*, suggesting an independent regulation pathway. We then considered the top-100 most
176 expressed genes in WT within the lists of *gat5Δ,* or *hap2Δ* downregulated genes reasoning that the

177 impact of a gene downregulation associated with a mutation would have a phenotypic consequence
178 if this gene is strongly expressed in the WT strain. Interestingly, 21 of the 39 previously identified *C.*
179 *neoformans* enriched EV-protein encoding genes[14] were regulated by either *GAT5* or *HAP2* (**Fig. 4E**).
180 In addition, the 15 genes coding for EV proteins regulated by both TFs included seven proteins
181 belonging to the top ten most abundant EV-associated proteins in *C. neoformans*. Thus, *HAP2* and
182 *GAT5* regulate the expression of many EV-associated protein components, confirming their function
183 as major regulators of EV production in *C. neoformans*.

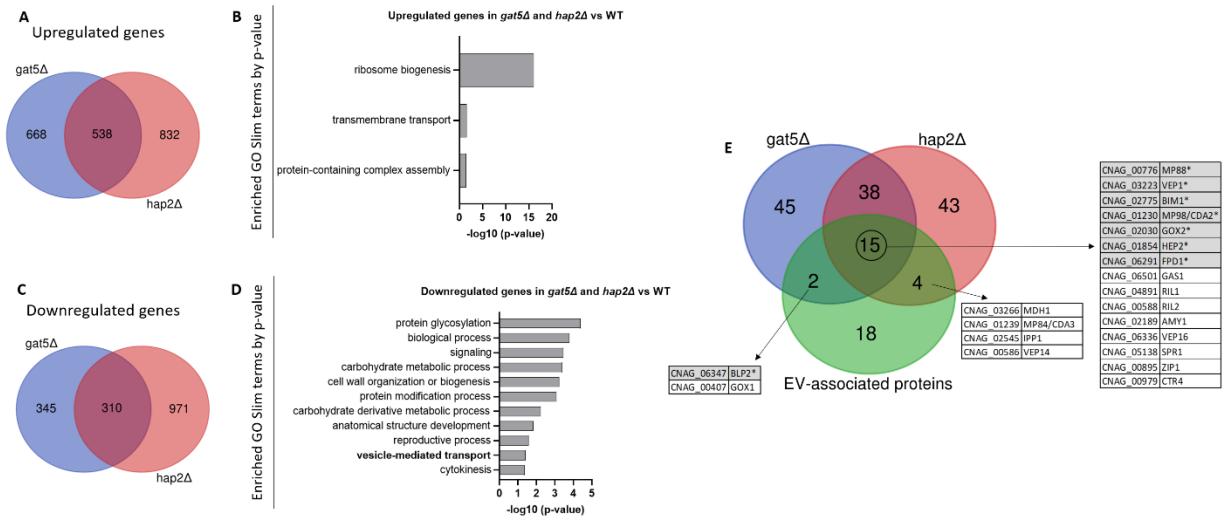

184

185 **Figure 4:** Transcriptomic analysis of the EV-deficient mutants *hap2Δ* and *gat5Δ* grown in EV-producing conditions. Venn
186 diagram revealing the number of upregulated genes in both mutants (A). Analysis of the GO SLIM categories enriched in the
187 group of genes upregulated in both mutants (B). Venn diagram revealing the number of the downregulated genes in both
188 mutants (C). GO SLIM categories enriched in the group of downregulated genes in both mutants (D). Venn diagram revealing
189 the overlap between genes downregulated in *gat5Δ* and *hap2Δ*, and the ones coding for the EV-enriched proteins of *C.*
190 *neoformans*, previously identified by proteomics (E). The genes highlighted in grey with an asterisk encode proteins among
191 the ten most abundant proteins in *C. neoformans* EVs.
192
193

194 **d) EV production regulator mutant strains are altered in azole susceptibility**

195 Strikingly, all four newly identified EV production mutant strains have been reported to have
196 altered FLC sensitivity in the systematic phenotypic analysis of the TF mutants published by the Bahn's
197 laboratory[25]. Indeed, we confirmed that *hap2Δ*, *gat5Δ,* and *liv4Δ* were less susceptible to FLC, while
198 *bzp2Δ* was more susceptible compared to the WT strain (**Fig 5A-B**). Similar phenotypes were observed
199 with Itraconazole and Voriconazole (**Fig 5A**). We also tested the FLC susceptibility of the *hap* mutants
200 and noticed that those impaired in EV production (i.e., *hap2Δ*, *hap3Δ,* and *hap5Δ*) were also more
201 resistant to FLC. In contrast, the *hapXΔ* mutant strain only displayed slight differences in FLC sensitivity
202 or no alteration in EV production (**Fig 5C-D**).

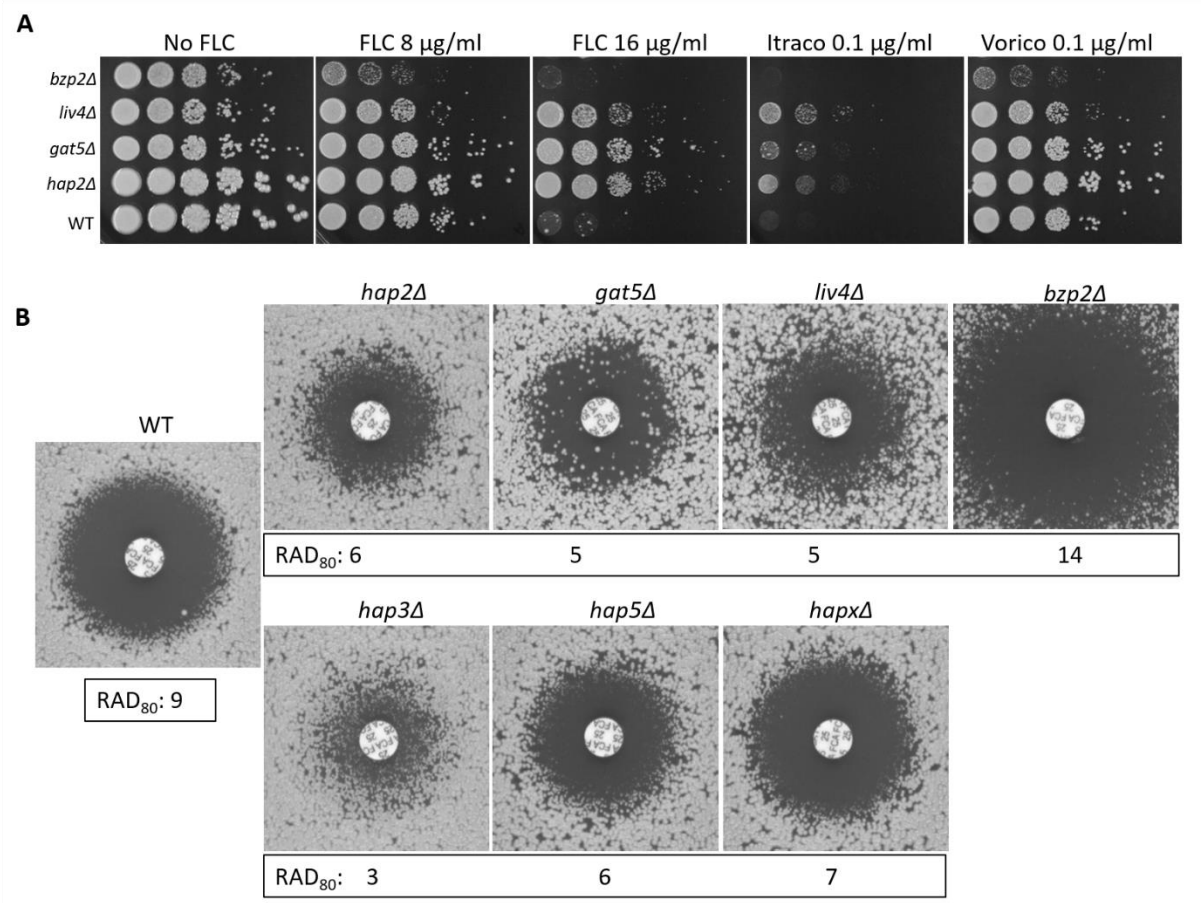


**Figure 5:** Transcription factors regulating EV release are associated with altered azole susceptibility. Spot assay for Fluconazole (FLC), Itraconazole (Itraco) and Voriconazole (Vorico) susceptibility (A) and FLC diffusion disk diffusion assay (25 µg/disk) for the four EV-defective TF mutants identified in the screening (*hap2Δ*, *gat5Δ*, *liv4Δ* and *bzp2Δ*), and for all the members of HAP complex inlcuing *hap3Δ* , *hap5Δ* and *hapXΔ,* grown for 72h (B). Average $RAD_{80}$ values obtained from diskImageR analyses are provided. The results are illustrative of three biological replicates.

Accordingly, reconstruction of the *gat5Δ* and *hap2Δ* mutant strains restored both phenotypes to WT levels (**Fig 6A-D**). We also evaluated the sensitivity of these strains to agents that disturb the cell wall and plasma membrane, such as Calcofluor white - CFW, hydrogen peroxide - $H_2O_2$, and sodium dodecyl sulfate – SDS, and observed that only *gat5Δ* was more susceptible to the presence of SDS (**Fig 6E**). Overall the analysis of TF mutant strains suggested that EV production and FLC susceptibility are coregulated.

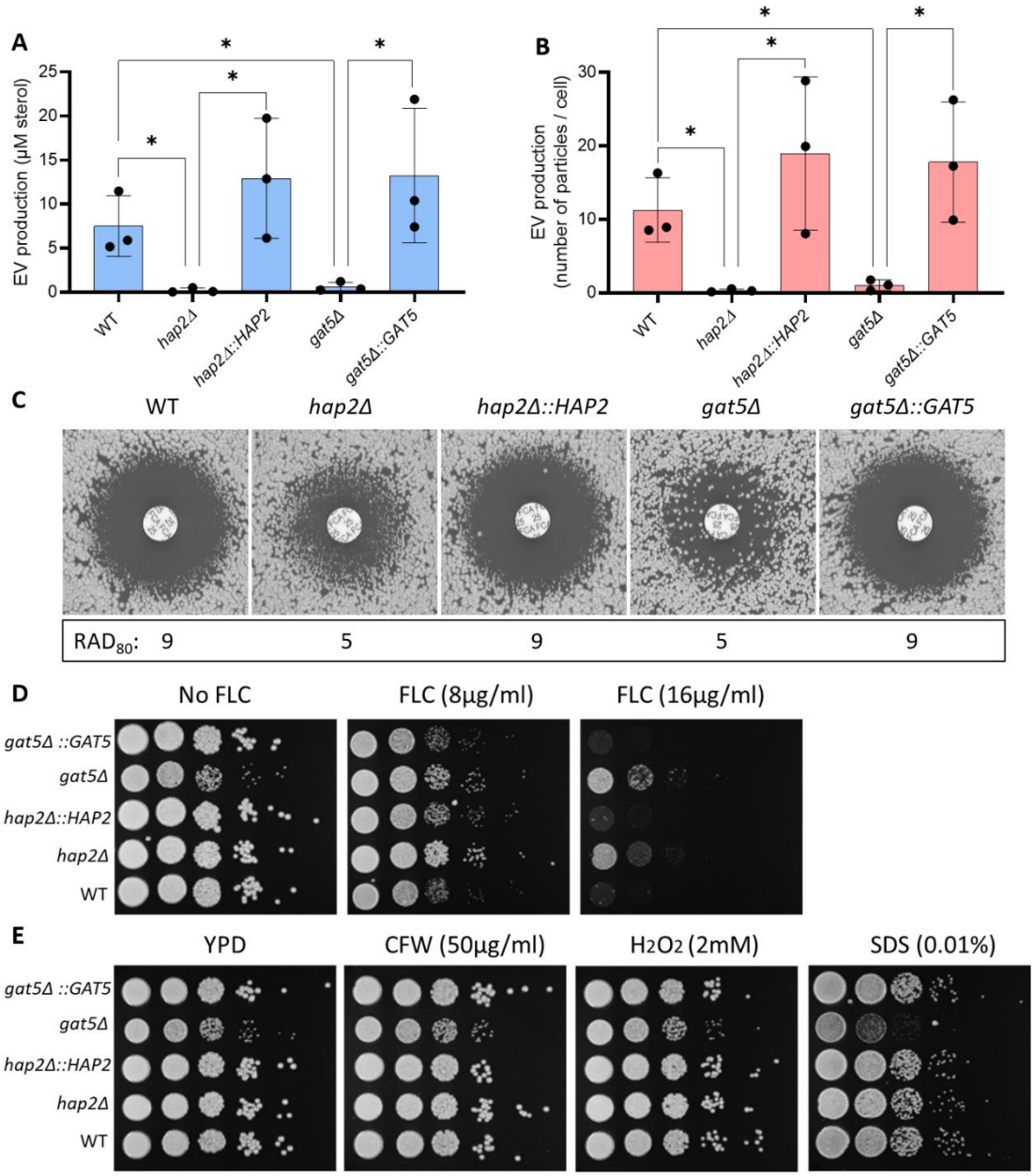


**Figure 6:** Complementation of the *hap2Δ* and *gat5Δ* mutant strains restores the phenotypes of EV production and FLC susceptibility. Total sterol contents in EVs produced by WT, mutants, and complemented cells. Sterol concentrations were normalized to the number of cells in each culture (A). Quantification of EV particles using nanoFCM in WT, mutants and complemented strains (B). FLC susceptibility by disk diffusion assay (25µg/disk) and $RAD_{80}$ values obtained by diskImageR (C). FLC susceptibility analysis by spot assay (D). Growth analysis in the presence of cell wall and plasma membrane disturbing agents (Calcofluor White - CFW, Hydrogen Peroxide - $H_2O_2$, and Sodium Dodecyl Sulfate - SDS). The experiments were carried out in biological triplicates. Error bars show means ± SD.

### e) *hap2Δ* FLC resistance is not associated with *ERG11* or *AFR* genes over expression

In *C. neoformans,* FLC resistance has been associated with either mutation of *ERG11* (CNAG_00040) and/or the overexpression of efflux pumps genes such as *AFR1* (CNAG_00730)*, AFR2* (CNAG_00869) and *AFR3* (CNAG_06909)[30]. Interestingly, differential gene expression analysis of *gat5Δ*, *hap2Δ,* and WT cells grown under conditions of EV production revealed that neither mutation was associated with an increased expression of any of these resistance genes. We then used RT-qPCR

231 assays to evaluate the expression levels of *ERG11* and the *AFR* genes in the presence or absence of
232 FLC in these genetic backgrounds. As an additional control, we also included a strain lacking *NRG1*
233 (CNAG_05222), which was shown to be FLC resistant[25] but was found here to produce WT EV levels
234 (**Fig S2**). In the absence of FLC, we did not observe changes in *ERG11* expression associated with either
235 *HAP2* or *GAT5* deletion (**Fig 7A**). In the presence of the drug, the expression of *ERG11* in the *hap2Δ*
236 mutant strain was similar to the WT, whereas in *gat5Δ*, we observed a two-fold reduction expression.
237 In contrast, in the *nrg1Δ* mutant strain, we observed a two-fold overexpression of *ERG11* as compared
238 to the WT strain. Thus, the FLC resistance phenotype in *hap2Δ* and *gat5Δ* mutants cannot be explained
239 by an alteration in *ERG11* expression levels (**Fig 7A**).
240 In contrast to *ERG11*, the presence of FLC did not impact the expression of *AFR* genes in any of these
241 strains (**Fig 7B–C–D**). However, *AFR1* and *AFR3* but not *AFR2* were upregulated in the *gat5Δ* mutant
242 (both with and without FLC), suggesting that these two efflux pumps could play a role in driving FLC
243 resistance in this strain (**Fig 7B–C–D**). A similar result was obtained with the *nrg1Δ* mutant, although
244 to a lesser extent for *AFR3*. Interestingly, in the *hap2Δ* strain, the expression of the *AFR* genes was

245 not altered, suggesting that additional mechanisms are driving FLC resistance in these cells.

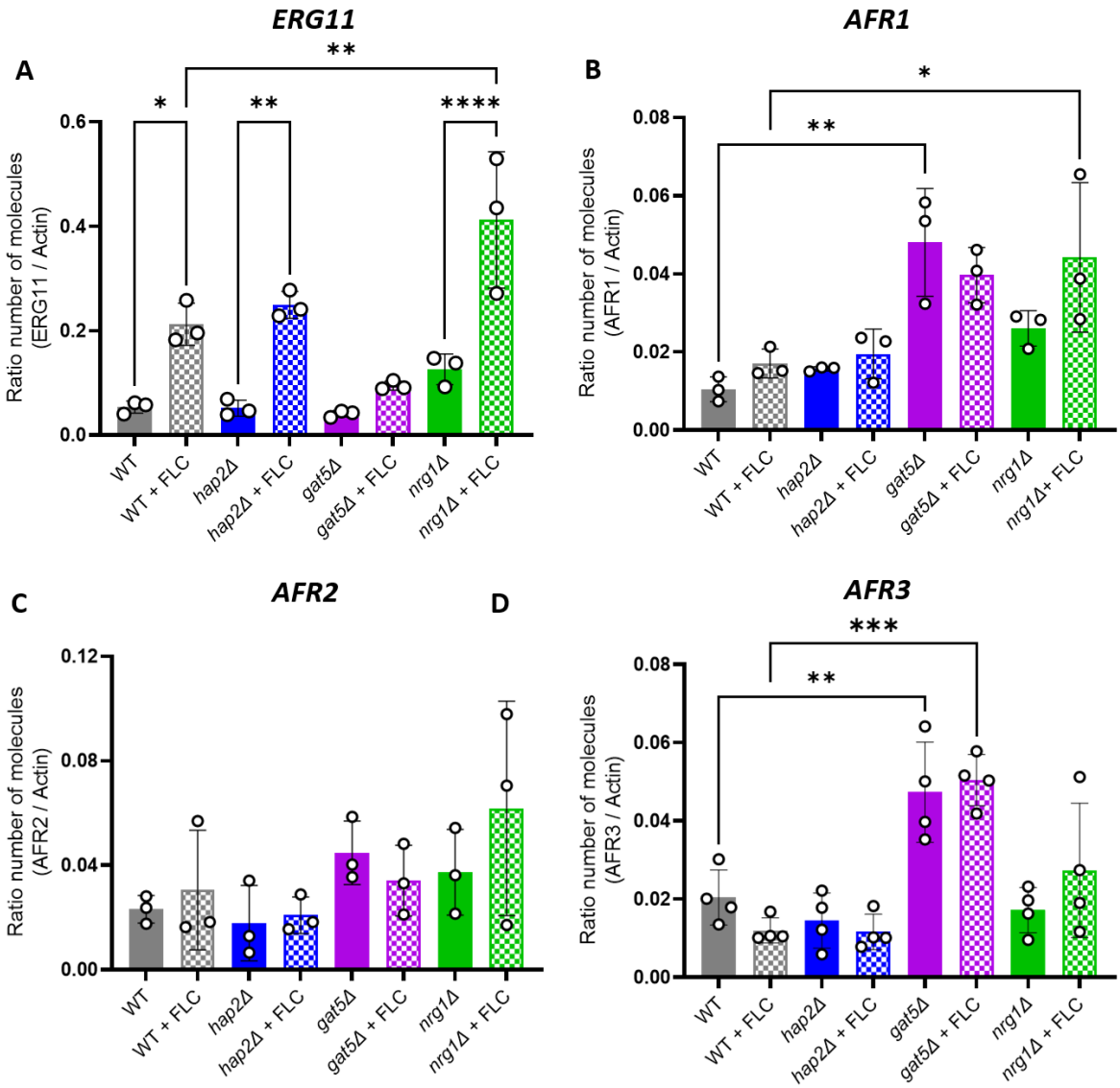


246

247 **Figure 7:** Gene expression analysis of known FLC resistance regulators in *C. neoformans*. *ERG11* (A), *AFR1* (B), *AFR2* (C), and
248 *AFR3* (D) gene expression profile as generated by RT-qPCR. The experiments were carried out in at least biological triplicates.
249 Error bars show means ± SD.

250

251 **f) FLC regulates EV production and cellular lipid profile**

252 The analysis of the EV regulators suggests that changes in EV production impact FLC resistance.
253 We then studied the converse relationship and tested whether FLC could modulate EV production in
254 *C. neoformans*. We first tested the growth of WT cells on SD containing FLC at different concentrations
255 (0.3, 0.6, 1.25, 2.5, and 5 µg/mL) identifying 0.6 µg/mL as the highest FLC concentration, which was
256 not affecting cellular growth (**Fig 8A**). At this concentration, the expression of *ERG11* was not altered
257 (**Fig 8B**). However, EV production was reduced by 2.4-fold (**Fig 8C**), suggesting that FLC regulates EV
258 production levels.

FLC is an inhibitor of the Erg11 lanosterol 14-demethylase, which transforms lanosterol in 4,4-dimethyl-cholesta-8,14,24-trienol in the fungal ergosterol biosynthetic pathway[31]. We thus compared the cellular lipid profile in WT and EV-defective mutant cells in the presence or absence of the same FLC-subinhibitory concentration (0.6 µg/mL). As expected[32], FLC treatment led to lanosterol accumulation in all strains under the growth conditions examined **(Fig 8D)**. However, decreased accumulation was observed in the *gat5Δ* and *hap2Δ* mutant strains as revealed by the ratio of lanosterol/ergosterol signals, suggesting that the lipid composition is altered in these EV-defective strains (**Fig 8E**).

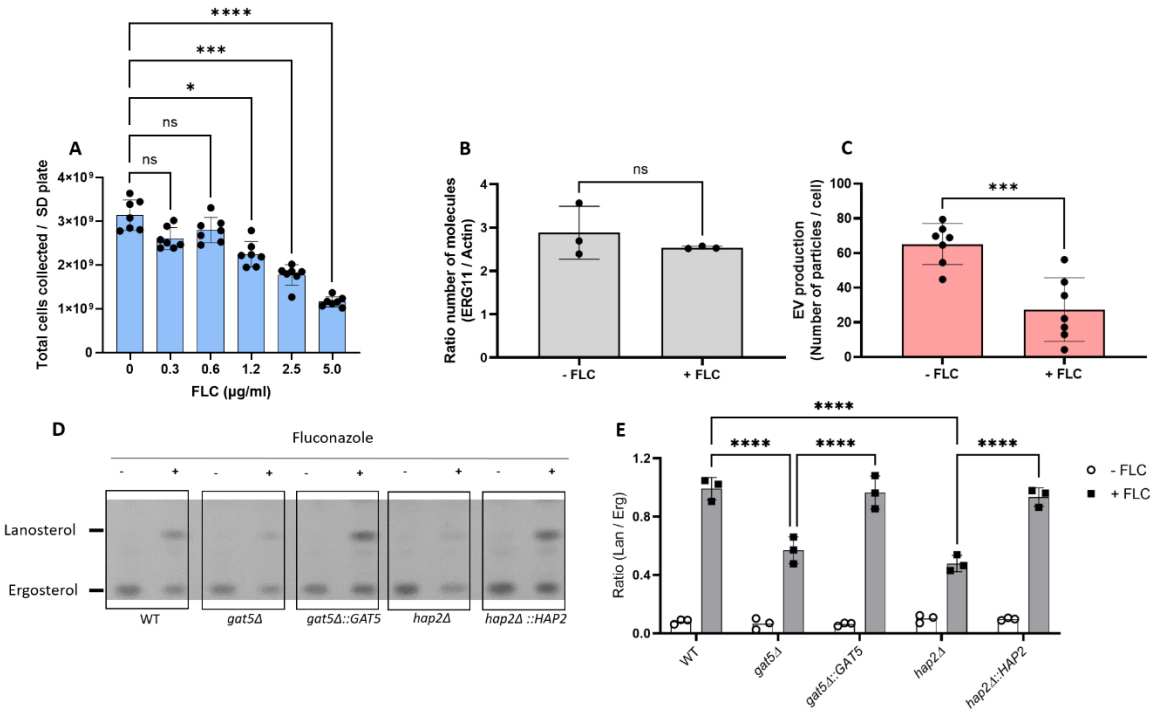


**Figure 8:** Fluconazole treatment affects EV production and cellular sterol homeostasis. WT cells were grown in different concentrations of FLC on SD agar medium, and the total number of cells was counted (A). Levels of *ERG11* expression in the presence of a subinhibitory concentration of FLC (0.6 µg/mL) (B). Analysis of EV production by nanoFCM in the presence of FLC (0.6 µg/mL) (C). Analysis of Lanosterol and Ergosterol lipid profile by thin layer chromatography, TLC in cells (D). Analysis of TLC bands by densitometry units and ratio between lanosterol and ergosterol-specific signals for cells (E). The experiments were carried out in at least biological duplicates, and representative results were shown. Error bars show means ± SD.

### g) FLC-resistant isolates obtained *in vitro* are impaired in EV production

To further explore the link between FLC resistance and EV production in *C. neoformans*, we analysed the EV production in spontaneous FLC-resistant isolates obtained *in vitro*. Previous studies reported that when *C. neoformans* cells are spread on a medium containing an inhibitory FLC concentration, a subset of the cell population can grow and produces colonies. This phenomenon is known as heteroresistance and was associated with the duplication of chromosome 1 bearing *ERG11* and *AFR1* resistance genes[12,33,31]. This FLC-resistant phenotype can be reverted by subculturing the cells in a drug-free medium, the phenotypic reversion being associated with the reversion of the

283 aneuploid genotype[11]. Therefore, we isolated independent spontaneous FLC-resistant colonies on
284 plates containing 15 µg/mL of FLC. FLC-susceptible parental and FLC-resistant isolates were then
285 passaged six times in a liquid drug-free YPD. A schematic overview of the experimental design is
286 delineated in **Fig 9A.** All parental, resistant, and passage strains were tested for EV production and
287 FLC sensitivity. As expected, the sixteen "passage 0" strains isolated on plates containing FLC were
288 resistant to FLC, as revealed by a significant decrease in the inhibition halo in FLC-disk diffusion assays
289 (**Fig 9B** and **9D**). Interestingly, this drug-resistant phenotype was accompanied by a substantial
290 reduction in EV production as analysed by nano-FCM (**Fig 9C**). Importantly, none of the sixteen FLC-
291 resistant isolates had pronounced growth defects in the SD medium, presenting the same transition
292 time frame from the exponential to stationary phase (**Fig S3**). In contrast, the "passage 6" strains all
293 lost their resistant phenotype, although to a different extent (**Fig 9E** and **9G**), and they also restored
294 EV production to parental levels (**Fig 9F**).

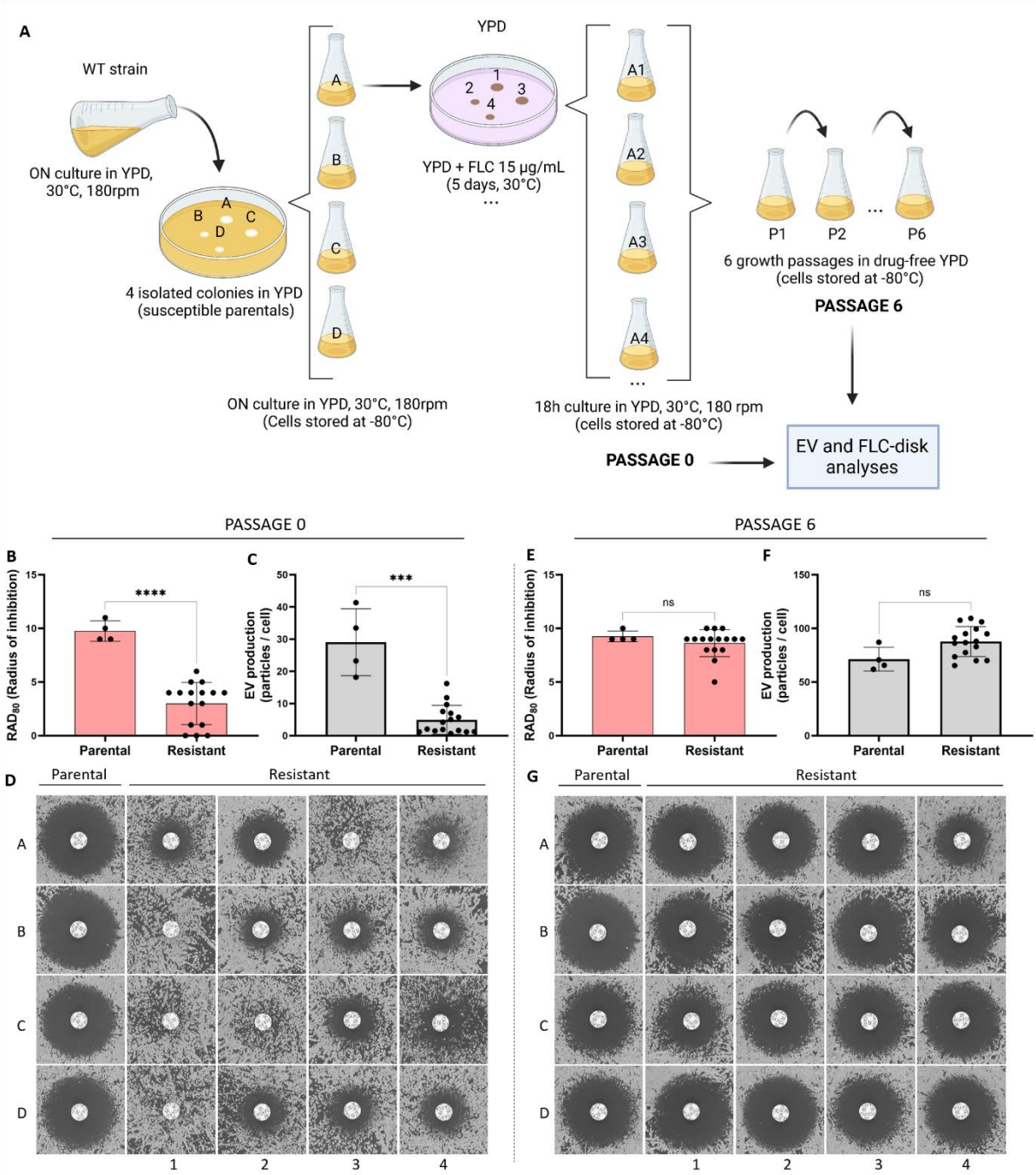


**Figure 9:** Analysis of FLC susceptibility and EV production in FLC-resistant isolates obtained *in vitro*. Illustrative scheme of the experimental strategy used to explore the association between FLC resistance and EV production in spontaneous drug-resistant strains obtained *in vitro* (A). Cells at passage 0: quantitative analysis of the growth inhibition halo from the FLC-disk diffusion assays by diskImageR, $RAD_{80}$ (B), EV production analysis by nanoFCM (C), and qualitative analysis of the inhibition halo of the FLC-disk diffusion assays (D). Cells after six successive passages in the absence of FLC: quantitative analysis of growth inhibition halo from the FLC-disk diffusion assays by diskImageR, $RAD_{80}$ (E), EV production analysis by nanoFCM (F), and qualitative analysis of the growth inhibition halo (G). Schematic representation created in BioRender.

We then evaluated the chromosome copy numbers of the parentals, FLC-resistant, and passaged strains first by qPCR assays using primers specific to genes located on chromosome 1 left arm (CNAG_00047), chromosome 1 right arm (CNAG_00483) and chromosome 2 (CNAG_03602). As expected, all four parentals were monosomic for chromosome 1 (**Fig 10A and 10D**). In agreement with

308 the published literature, we also found that fourteen out of sixteen FCL-resistant strains were disomic
309 for chromosome 1 (**Fig 10B** and **10E**). Meanwhile, all "passage 6" strains reverted to the original
310 monosomic state of chromosome 1 (**Fig 10C** and **10F**).

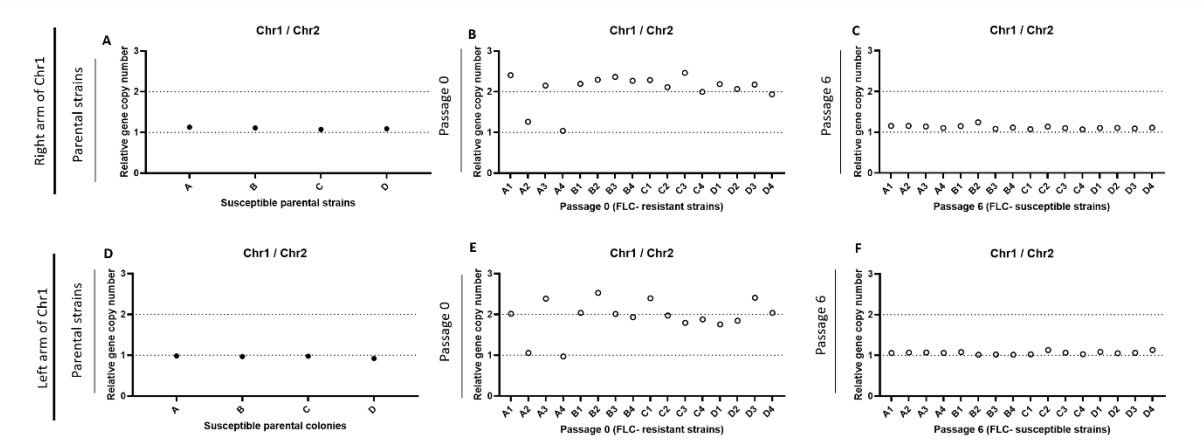


311

312 **Figure 10**: qPCR assays evaluating the monosomic or disomic status of chromosome 1 in the FLC sensitive and resistant
313 strains obtained *in vitro*. Parental strains (A and D), FLC-resistant "passage 0" strains (B and E), and "passage 6" strains (C and
314 F) were tested using primers specific for genes located on chromosome 1 right (A to C) and left arms (D to F). Primers specific
315 to chromosome 2 were used as control.

316

317 Because qPCR analysis suggested that the two FLC-resistant strains A2 and A4 were
318 monosomic for chromosome 1, we sequenced the genomes of the A series to examine possible
319 alternative copy number variations in these strains. This analysis confirmed that strains A1 and A3
320 were disomic for chromosome 1, while strains A2 and A3 were disomic for chromosome 4 (**Fig 11A**).
321 The FLC-resistant strain A4 showed no chromosome duplication but an increase in the
322 mitochondria/nuclear genomes ratio, which reverted simultaneously with the FLC-resistance
323 phenotype in the corresponding passage strain (**Fig 11A and Fig 12A**). The same was observed in the
324 A2 and A3 series, in which the FLC-resistant strains displayed an increase in mitochondria genome
325 copy number, which was reverted in the FLC-sensitive passage strains (**Fig 11A**). Although we did not
326 investigate further whether these two observed phenomena share a causative linkage, genome
327 sequencing of the *gat5Δ* mutant grown under EV-producing condition also revealed increased
328 numbers of mitochondria (**Fig 12B**).

329 Interestingly, while *ERG11* but not *AFR1* was overexpressed in the P0_A2 isolate, we found no
330 change in the expression of these resistance genes in the P0_A4 isolate, suggesting that its FLC-
331 resistant phenotype was independent of their regulation (**Fig 11B-C**).

332

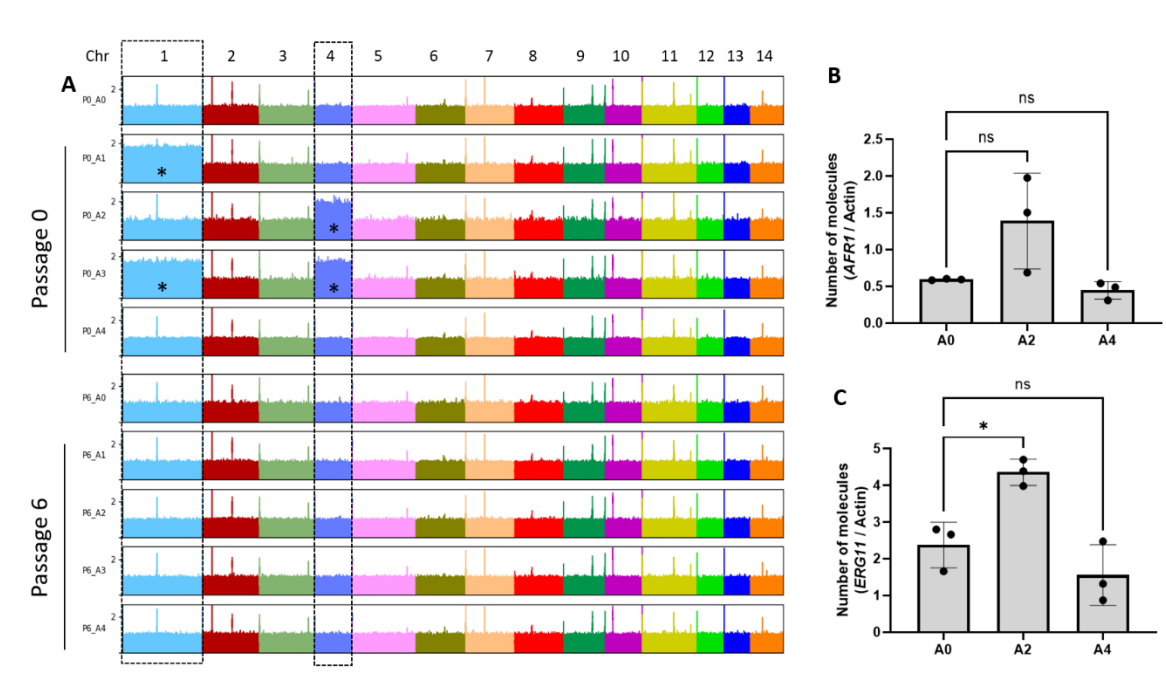


**Figure 11:** Chromosome duplications revealed after aligning DNA sequencing reads obtained from the A series of strains to the *C. neoformans* reference genome (A). Analysis of *AFR1* (B) and *ERG11* (C) gene expression in A0, A2, and A4 strains by RT-qPCR. Indicative of chromosome duplication (*).

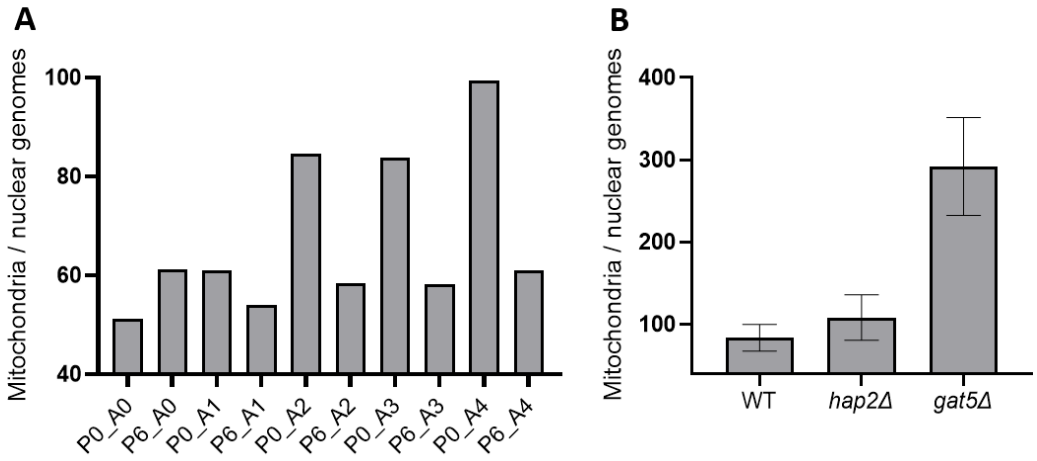


**Figure 12:** Analysis of mitochondria/nuclear genome ratios in *C. neoformans* isolates obtained *in vitro* (A) and in EV-defective mutant strains (B). P0: growth passage 0, P8: growth passage 8. A0 is the parental strain, and A1 to A4 are the FLC-resistant strains derived from A0. A1-A4 lost the FLC-resistance phenotype after eight growth passages in the absence of FLC.

### h) FLC resistance and regulation of EV release in *C. neoformans* clinical isolates

To test whether the relationship between EV production and FLC resistance would extend to clinical isolates, we studied a series of isolates having different levels of FLC susceptibility. Plotting the the radius of inhibition ($RAD_{80}$) from FLC-disk diffusion assays and the average levels of EV production from these isolates did not reveal a clear correlation ($R^2 = 0.002$), as both the fully resistant isolates (no inhibition halo), as well as the most sensitive ones, were poor EV producers (**Fig 13A**). We then

349 considered serial isolates of *C. neoformans* that had become resistant during infection. For the isolates
350 CNRMA17.247 and CNRMA20.738, we observed that the acquisition of FLC resistance coincided with
351 the decreased ability to produce EVs (**Fig 13B**). For the second lineage (isolates CNRMA4.1291 and
352 CNRMA4.1293), we did not observe any difference in EV production between the sensitive and the
353 resistant isolates (**Fig 13C**). Interestingly, SNPs analysis revealed a CNRMA4.1293 specific (A to T)
354 nonsynonymous mutation within the *ERG11*, responsible for a Y145F mutation and possibly associated
355 with the acquired resistance[34]. We then tried to revert the resistance phenotype of four FLC-resistant
356 clinical isolates (CNRMA20.738, CNRMA4.1293, CNRMA4.158, and CNRMA5.114) by growing them in
357 a drug-free YPD medium for eight subsequent passages. CNRMA5.114 was the only isolate for which
358 we obtained a more sensitive derivative (**Fig 13D**). In agreement with our previous observation, the
359 P8-sensitive passage produced more EVs than the original P0-resistant isolate (**Fig 13E**). As expected,
360 P8 strains with no change in drug susceptibility also did not display altered EV production (**Fig 13D-E**).
361 We then sequenced the genome of the two lineages of recurrent isolates as well as the P0 clinical
362 isolates and their P8 derivatives. We observed no large genome duplication of the recurrent clinical
363 isolates (**Fig S4**). Among the sequenced P0 clinical isolates, we observed the whole chromosome
364 duplication of chromosome 12 in CNRMA5.114, which was lost in its P8 sensitive derivative. Partial
365 duplication of chromosome 14 was also observed in the reverted passage 8 strain (**Fig 13F**). Again, we
366 did not further investigate a possible causative link between FLC resistance and the observed genotype
367 modifications in these isolates.

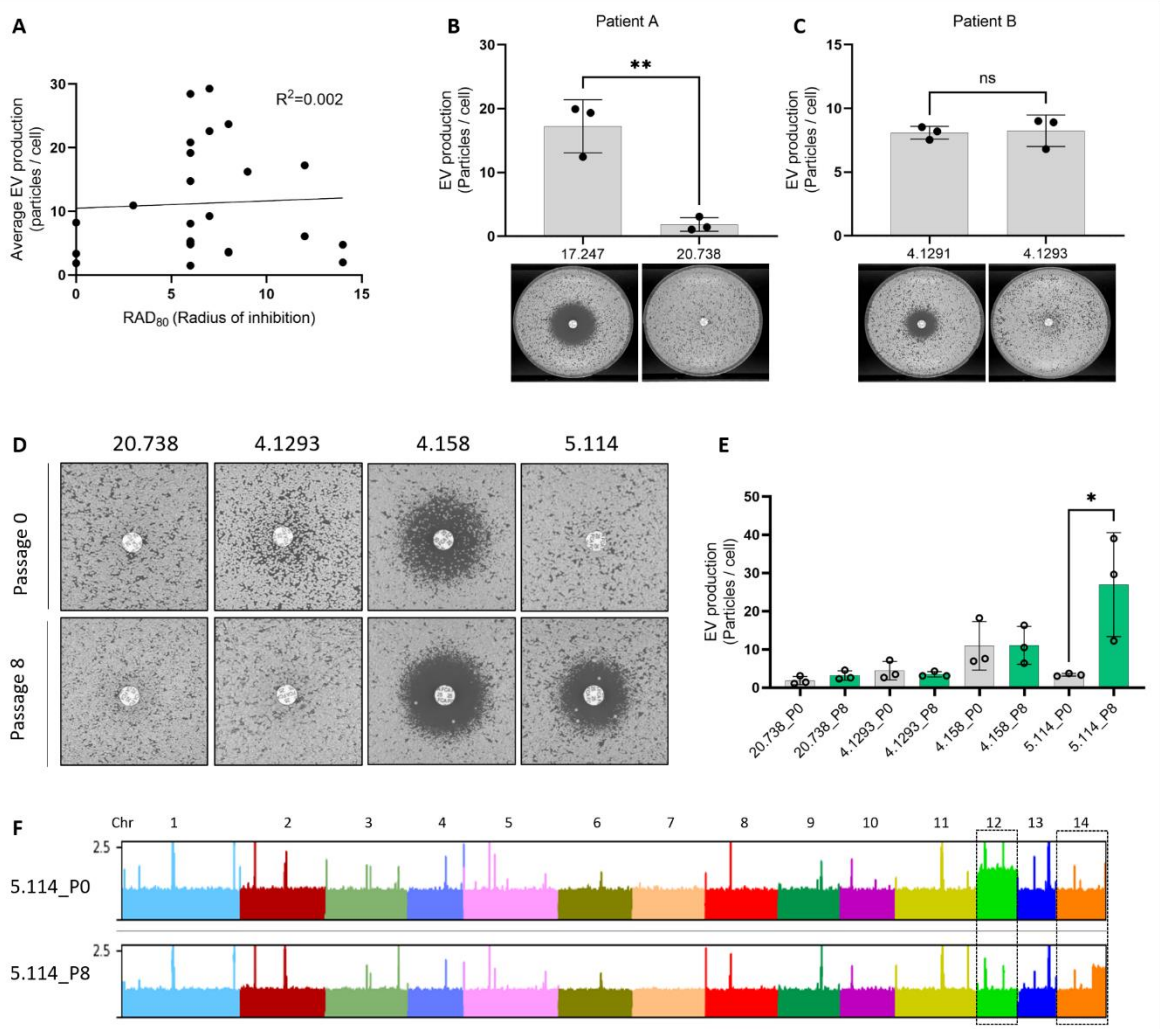


**Figure 13: EV production and FLC resistance are linked in clinical isolates.** Analysis of EV production by nanoFCM and size of FLC-disk inhibition halo in clinical isolates by linear regression (A, radius of inhibition = $RAD_{80}$ values by diskImageR). EV production as measured by nanoFCM in the recurrent isolates CNRMA17.247 and CNRMA20.738 (top) and FLC-disk diffusion assays (bottom) from patient A (B). EV production as measured by nanoFCM in the recurrent isolates CNRMA4.1291and CNRMA4.1293 (top) and FLC-disk diffusion assays (bottom) from patient B (C). FLC-disk diffusion assay in passaged clinical isolates (D) and analysis of EV production of passaged clinical isolates by nanoFCM (E). Alignment of DNA-Seq reads obtained from P0, and P8 CNRMA5.114 passaged clinical isolates (F). EV and FLC-disk analyses were carried out in at least biological triplicates, and representative results were shown.

## 3) Methods

### Media and culture conditions.

All strains were taken from the G. Janbon laboratory collection at -80°C, plated onto yeast peptone dextrose (YPD) agar plates (1% yeast extract, 2% bacto-peptone, 2% dextrose, 2% bacto-agar) and incubated at 30°C for 48h before each experiment. Cell inoculum was performed in broth YPD (1% yeast extract, 2% bacto-peptone, 2% dextrose) rotating at 180 rpm for 24h at 30°C. The other solid media used in this study included Sabouraud (SAB) containing 1% bacto-peptone, 4% dextrose, 2% bacto-agar, Synthetic dextrose (SD) containing 0.67% yeast nitrogen base (Difco) without amino acids,

386 2% glucose and 2% bacto-agar; and Capsule induction medium (IM) containing 1.7 g of yeast nitrogen
387 base without amino acids and without ammonium sulfate (Difco), 1.5 g of asparagine and 20 g of
388 glucose $L^{-1}$ of buffer (12mM in $NaHCO_3$, 35mM in MOPS, pH 7.1), as previously described[35]. Drug-
389 containing plates were made by adding a stock solution of 3 mg/mL FLC powder in water~~,~~ to different
390 final concentrations depending on each experiment. The drug was added to the agar after autoclaving,
391 then cooled to approximately 50°C before pouring.
392
393 **Fungal strains and mutant construction**
394 The *C. neoformans* TF mutant library[26] was obtained from the Fungal Genetic Stock Center (USA). This
395 collection has been constructed in an H99o background[36]. After the screening, the phenotype of the
396 identified EV mutant strains was thus confirmed in the KN99α[37] background. All the following
397 experiments have been performed in KN99α reference background[36]. The strains used are listed in
398 **Supplementary Table S2**. The strains *MATα hap2Δ::NAT* (CNAG_07435), *MATα hap3Δ::NAT*
399 (CNAG_02215), *MATα hap5Δ::NAT* (CNAG_07680), *MATα hapXΔ::NAT* (CNAG_01242), *MATα*
400 *gat5Δ::NAT* (CNAG_05153), *MATα nrg1Δ::NAT* (CNAG_05222) have been constructed in the Hiten
401 Madhani lab (UCSF, USA) and obtained from the Fungal Genetic Stock Center. The genotypes of these
402 mutant strains were confirmed by PCR using gene-specific internal primers. To construct the strains
403 NE1539 (*MATα bzp2Δ::NAT*) and NE1540 (*MATα liv4Δ::NAT*), we replaced the entire CNAG_04263
404 (*BZP2*) and CNAG_06283 (*LIV4*) CDS by the NAT marker. The deletion cassettes construction and
405 transformant screening were performed as previously described[33]. The *GAT5* and *HAP2* genes were
406 re-introduced into the corresponding mutant strain using a transient CRISPR-Cas9 expression (TRACE)
407 system[38]. DNA fragments spanning a genomic region from 1kb upstream to 1kb downstream the CDS
408 of the genes were PCR amplified and cloned into the pSDMA57 plasmid before being integrated at the
409 genomic "safe haven" locus in *gat5Δ* and *hap2Δ* mutants, repectively[39]. All plasmids and primer
410 sequences used are provided in **Supplementary Tables S3 and S4**, respectively. Twenty-four clinical
411 isolates of *C. neoformans* were also used. All isolates were recovered from the national cryptococcosis
412 surveillance program managed by the National Reference Center for Invasive Mycoses & Antifungals
413 (NRCMA, Institut Pasteur) between 2004 and 2021. All the clinical isolates and respective MIC values
414 are provided in **Supplementary Table S2.**
415
416 **EV isolation protocol and optimization for EV screening in 96-well plates**
417 EV isolation by the conventional ultracentrifugation method followed the steps of the previously
418 described protocol[14]. A 96-format protocol was also used to test a large number of samples
419 concomitantly. For this, cells from the stock were steacked on YPD agar plates for 48h at 30°C, and

420 one loop of cells was inoculated in 1 ml of YPD broth of each well of a 96-deep well plate and incubated
421 for 18h at 30°C under agitation. The plate was centrifuged, and cells were washed twice with sterile
422 water, adjusted to $OD_{600}$ = 0.4 using a Tecan microplate reader (Tecan Trading AG, Switzerland). Then,
423 300 µL of the cell suspension was spread onto SD agar plates. After incubation for 24h at 30°C, cells
424 were gently recovered from the agar plates with an inoculation loop and suspended in 1 mL of 0.22
425 µm-filtered PBS 1x in 2 mL Eppendorf tubes by pipetting up and down. The total number of cells
426 collected from plates was evaluated by Coulter Counter (Z series, Beckman). Cells were centrifuged
427 for 5 min at 7,000 x *g*; the supernatant was collected in a 1.5ml tube and centrifuged again at 11,000
428 x rpm for 5 min. Supernatants were transferred to 96-well filter plates with 0.45 µm pore size and
429 centrifuged at 2,500 x g for 3 min at 4°C. The filtered supernatants were kept at -80°C for further
430 evaluations, including the quantification of EV single particles and EV size diameter by the Flow
431 Nanoanalyser[40] (nanoFCM™) and/or by measuring the total sterol amount by Amplex™ Red
432 Cholesterol Assay Kit (ThermoFisher, A12216), following manufacturer's instructions.
433 In the TF mutant collection[25], each mutant is present as two or three independently obtained
434 strains. Here, we first tested one mutant per gene. We then selected the most promising candidates
435 producing less than 0.5-fold or more than 1.5-fold EVs compared to the WT strain. We then tested the
436 second and third independent mutants when available in the collection. For all the mutants tested,
437 the EV production was measured by the total amount of sterol normalized by the total number of cells
438 collected for each strain. For the mutant strain 3.C10 (*gat1Δ*), which did not grow on SD plates, the EV
439 production ratio was calculated based on mutant and WT growth on YPD agar plates.
440
441 **Quantification of EV particles by nanoFCM**
442 A NanoAnalyzer (nanoFCM) instrument equipped with a 488 nm laser at 50 mW and single-photon
443 counting avalanche photodiodes detectors (SPCM APDs) was used for the detection of the EV
444 particles. Band-pass filters allowed for the collection of light in specific channels (488/10 nm). Light
445 scattering and fluorescence of individual EVs were collected on single-photon counting avalanche
446 photodiodes detectors on three channels: side scatter (SSC) - 488/10 (trigger channel). Sample fluid
447 was focused to approximately 1.4 µm using an HPLC-grade water filter and de-gas as the sheath fluid
448 via gravity feed. Data were generated through the Nanoanalyser Professional Suite V 2.0 software,
449 0.02 µm- filtered PBS was used to define the event triggering threshold. Measurements were taken
450 over one-minute periods at a sampling pressure of approximately 1.0 kPa, modulated, and maintained
451 by an air-based pressure module. Samples were diluted in 0.02 µm- filtered PBS as required to allow
452 3,000 to 13,000 counts to be recorded during this time. During data acquisition, the sample stream is
453 completely illuminated within the central region of the focused laser beam, resulting in approximately

454 100% detection efficiency, which leads to accurate particle concentration measurement via single-
455 particle enumeration. Optical alignment was tested and calibrated using fluorescent 250 nm silica
456 nanoparticles.Further calibration measurements were taken prior to analysis using 250 nm silica
457 nanoparticles of known concentration (for EV concentration calculation). Isolated EV samples were
458 sized according to standard operating procedures using the proprietary 4-modal silica nanosphere
459 cocktail generated by nanoFCM to allow for a standard curve to be generated based on the four sizes
460 of the nanosphere populations of 68 nm, 91 nm, 113 nm, and 155 nm in diameter. Silica provides a
461 stable and monodisperse standard with a refractive index of approximately 1.43 to 1.46, which is close
462 to the range of refractive indices reported in the literature for EVs ($n$ = 1.37 to 1.42). Using such a
463 calibration standard enabled accurate flow cytometry size measurements, as confirmed when
464 comparing flow cytometry with cryo-TEM results. The laser was set to 10 mW and 10% SSC decay.
465 Data reported in the figure were handled within the nanoFCM Professional Suite v2.0 software to
466 analyse particles between 40 nm and 155 nm.

467

468 **DNA and RNA purification and sequencing libraries preparation**

469 *C. neoformans* KN99α, *hap2Δ,* and *gat5Δ* strains were grown in EV production condition on SD for 18h
470 at 30°C. Cells were collected from the agar plates and suspended in 10ml 0.22µm-filtered PBS 1x. RNA
471 extracts were prepared as previously described[41,42]. Each condition was used to prepare biological
472 triplicate samples. RNA-seq analysis was performed as previously described[43]. Briefly, strand-specific,
473 paired-end cDNA libraries were prepared from 1.5 µg of total RNA by polyA selection using the TruSeq
474 Stranded mRNA kit (Illumina) according to the manufacturer's instructions. cDNA fragments of ∼400
475 bp were purified from each library and confirmed for quality by Bioanalyzer (Agilent). DNA-Seq
476 libraries from 2.5 µg of genome DNA were prepared using the TruSeq DNA PCR-free kit (Illumina).
477 Then, 100 bases were sequenced from both ends using an Illumina NextSeq500 instrument according
478 to the manufacturer's instructions (Illumina). ~~For genomic analyses, 50 bases were sequenced from~~
479 ~~one end using the same instrument.~~

480

481 **Sequencing library trimming and mapping**

482 The paired reads from the RNA-seq libraries were trimmed for low-quality reads, and Illumina TruSeq
483 adapters were removed with Cutadapt v1.9.1 (https://doi.org/10.14806/ej.17.1.200) with the
484 following parameters: --trim-qualities 30 –e (maximum error rate) 0.1 --times 3 --overlap 6 --
485 minimum-length 30. The cleaning of rRNA sequences was performed with Bowtie2 v2.3.3[44] with
486 default parameters; unmapped paired reads were reported using option --un-conc to identify reads
487 that did not align with rRNA sequences. The cleaned reads from RNA-seq paired-end libraries from *C.*

488 *neoformans* to the H99 reference genome (NCBI Genome Assembly GCA_000149245.3) with Tophat2
489 v2.0.14 [45] and the following parameters: minimum intron length 30; minimum intron coverage 30;
490 minimum intron segment 30; maximum intron length 4000; maximum multihits 1; microexon search.
491 Analysis of differential expression data was performed in DeSeq2[46].
492 DNA read alignment, variant detection, and ploidy analysis were performed as previously described
493 [47]. Illumina reads were aligned to the *C. neoformans* H99 reference genome using Minimap2 aligner
494 v.2.9[48] with the "-ax sr" parameter. BAM files were sorted and indexed using SAMtools[49] version 1.9.
495 Picard version 2.8.1 (http://broadinstitute.github.io/picard) tools were used to identify duplicate
496 reads and assign correct read groups to BAM files. SAMtools version 1.9 and Picard version 2.8.1 were
497 then used to filter, sort, and convert SAM files and assign read groups, and mark duplicate reads.
498 Single-nucleotide polymorphisms (SNPs) and insertions/deletions (indels) were called using Genome
499 Analysis Toolkit version 3.6 with ploidy=1 according to the GATK Best Practices. HaploScore
500 parameters used to filter SNPs and indels included VariantFiltration, QD <2.0, LowQD,
501 ReadPosRankSum<-8.0, LowRankSum, FS >60.0, HightFS, MQRankSum<-12.5, MQRankSum, MQ
502 <40.0, LowMQ, and HaplotypeScore >13.0. To examine variations in ploidy across the genome, the
503 sequencing depth at all positions was computed using SAMtools[49], and then the average depth was
504 computed for 1-kb windows across the genome. Gene ontology (GO) analyses were performed using
505 the FungiDB database (https://fungidb.org/fungidb/app).
506
507 **Obtention of FLC-resistant *in vitro* strains and passaged derivatives**
508 To obtain FLC-resistant *C. neoformans* strains *in vitro*, WT KN99α cells, previously grown for 24h at
509 30°C, were plated on drug-free YPD agar plates and incubated for 48h at 30°C. Four isolated parental
510 colonies were used to inoculate four YPD liquid cultures grown ON at 30°C. An aliquot of the cells was
511 stored at -80°C, and 1 ml of the culture was washed once with sterile water and adjusted to $10^5$
512 cells/mL. 200 µL of the cell suspension was plated on new YPD plates supplemented with FLC at
513 15µg/mL and incubated for five days at 30°C. Four independent FLC-resistant colonies for each initial
514 parental culture were collected from the plates, totalizing 16 resistant isolates. Each of these 16 strains
515 was cultured in liquid YPD drug-free medium ON before being stored at -80°C (P0 isolates). For the
516 culture passages, susceptible parental cells and FLC-resistant derived strains were thawed on YPD agar
517 plates (30°C) for 48h. One small loop of the cells was inoculated in 1 mL of YPD in 96 deep well plates
518 that were incubated under rotation at 30°C. Every 48h days, 10 µL of the cell suspension was collected
519 and inoculated in 990 µL of fresh YPD using a multichannel. The remaining cells from each passage
520 were centrifuged at 4000 x rpm for 5 min (4°C), the supernatant was discarded, and the cell pellet was
521 suspended in 200 µL of glycerol (40%) for keeping at - 80°C. Parental strains and 96 well plates

522 containing cells from passages 1 to 6 were stored at -80°C and further used for EV isolation and FLC-
523 disk assays.
524
525 **Disk diffusion and spot assays**
526 Disk diffusion assays were performed as previously described[42], with minor adjustments. Cells were
527 grown for 24h in YPD broth at 30°C under agitation, centrifuged, washed once in sterile PBS 1x, and
528 diluted at $1 \times 10^6$ cells/mL. 100µL of the cell suspension was spread onto YPD agar plates. A single 25
529 µg FLC disk (BioRad) was placed in the center of each plate. Plates were incubated at 30 °C for 48 h
530 and 72 h and photographed individually using a PhenoBooth+ (Singer Instrument, USA) apparatus.
531 Analysis of the disk diffusion assay was done by ImageJ or by using the diskImageR pipeline, as
532 previously described[50]. Radius of inhibition levels, referred to as RAD throughout the manuscript,
533 represents parameters measured at 80% drug inhibition ($RAD_{80}$). Cells for spot assays were prepared
534 following the same steps previously described. Cells were diluted to $1 \times 10^7$ cells/mL and spotted (3
535 µl) in 10-fold serial dilutions onto the YPD plates containing the different drugs and compounds. The
536 susceptibility assays were repeated a minimum of two times.
537
538 **RT-qPCR for *ERG11*, *AFR1-AFR3* expression, and chromosomal ploidy analysis**
539 For the analysis of gene expression by qPCR, three independent samples were prepared for each strain
540 (WT, *hap2Δ*, *gat5Δ,* and *nrg1Δ*). Cells were cultured in YPD for 18 h at 30°C, under agitation. Then , 6.4
541 x $10^8$ cells were transferred to 100 mL of YPD and grown for 4h, at 30°C, under agitation. After the 4 h
542 incubation, FLC was added at a final concentration of 10 µg/mL. We skipped this step in the control.
543 Cell cultures were incubated for 2 additional hours at 30°C under agitation. Cells were counted and
544 washed once with sterile water, and pellets were kept at -80°C for further RNA extraction, as
545 previously described[35]. Purified RNA was treated with DNase I recombinant, RNase-free (Roche) to
546 eliminate residual genomic DNA. Synthesis of cDNA was performed using the Thermo Scientific
547 Maxima First Strand cDNA Synthesis Kit for RT-qPCR, following the manufacturer's instructions. The
548 expression levels of *ERG11* and *AFR1-AFR3* genes were determined by qPCR using 5 µl of the
549 appropriate dilutions of cDNA and 1 µL of each primer of interest (10 µM), listed in **Supplementary**
550 **Table S4**. The reactions were performed using the SsoAdvanced Universal SYBR Green Supermix in
551 Hard Shell qPCR plate 96-well thin wall (Bio-Rad). Amplification reactions were performed using an
552 RT-PCR Detection System thermal cycler (Bio-Rad). The Ct values obtained in triplicates were
553 averaged, and the number of molecules measured by standard curves and normalized to that of the
554 housekeeping gene *ACT1* (CNAG_00483). All RT-qPCR data were from three biological replicates (three
555 independent RNA preparations).

556 We used qPCR assays and primers specific to the genes CNAG_00483, CNAG_00047, and CNAG_03602
557 to evaluate the copy number of the chromosome 1 right harm, chromosome 1 left harm, and
558 chromosome 2, respectively (**Supplementary Table S4**).
559
560 **Lipid analysis by thin layer chromatography**
561 Cells collected after 24h grown on SD agar plates with or without FLC (0.6µg/mL) were suspended in
562 a mixture of chloroform (C) and methanol (M), C/M (2:1 [vol/vol]) and incubated for 4h at room
563 temperature. The suspension was clarified by centrifugation, and the supernatants were stored. Cell
564 pellets were again extracted with a mixture of C and M (1:2 [vol/vol]) under the same conditions.
565 Supernatants containing the lipid extracts were combined and dried using a rotavapor (Heidolph,
566 Germany). The resulting cell lipid extracts were submitted to a partition system composed of
567 C/M/0.75% KCl in water (8:4:3 [vol/vol/vol]) and vigorously mixed. The lower phase was dried under
568 a $N_2$ stream, weighed, and suspended in C to reach a concentration of 10 mg/mL of total cellular lipid
569 extracted. To analyze cellular lipids, 50µg of total lipid was spotted into thin layer chromatography
570 (TLC) plates (silica gel 60 $F_{254}$; Merck, Germany). A total of 3 µL of purified Lanosterol and Ergosterol
571 (1mg/mL) were spotted in TLC plates as running standards. The plates were developed in chambers
572 pre-saturated for 10 min at room temperature using cyclohexane and ethyl acetate (3:2 [vol/vol] as a
573 solvent running system. Plates were sprayed with a solution of 50 mg ferric chloride ($FeCl_3$) in a
574 mixture of 90 mL water, 5 mL acetic acid, and 5 mL sulfuric acid. After heating at 100 °C for 3–5 min,
575 the sterol spots were identified by the appearance of a red-violet color. TLC plates were imaged, and
576 the bands were densitometrically analysed using Image J (NIH, USA). Values were expressed as ratios
577 between cellular lanosterol and ergosterol-specific levels.
578
579 **Statistical analysis**
580 All statistical analyses were performed using GraphPad Prism 9 software (GraphPad Software Inc.).
581 Data sets were tested for normal distribution using Shapiro-Wilk or Kolmogorov-Smirnov normality
582 tests. In the cases in which the data passed the normality test, they were further analysed using the
583 unpaired Student's t test or ordinary one-way ANOVA. When at least one data set was nonnormally
584 distributed, we used the nonparametric Kolmogorov-Smirnov or Kruskal-Wallis test.
585
586 **Availability and accession number**
587 Raw data are available at Bioproject: PRJNA928602
588
589 **4) Discussion**

590
591 The mechanisms of biogenesis of EVs in fungi are still unknown. In this paper, we present
592 experiments revealing a tight regulation of EV production in response to changes in growth conditions
593 in *C. neoformans,* confirming previous reports in other models[51,52]. We also characterize four
594 transcription factor mutant strains strongly impaired in EV production which are the first to be
595 described in fungi and, to our knowledge, in any organisms. Surprisingly, we observed no major growth
596 defect associated with *hap2Δ* mutation, suggesting that a WT level of EV production is dispensable in
597 this fungus, at least under the examined conditions.
598 Our experiments also indicate that EV production is also strongly regulated by fungal growth
599 phase. EVs are produced between 16 h and 22 h after cell plating, corresponding to the transition
600 between the exponential phase and stationary phase. This result was consistent with reports of cells
601 growing on YPD solid medium[52]. In *S. cerevisiae*, the transition from the exponential phase to the
602 stationary phase is associated with a shift from fermentation to respiration and a sharp slowdown of
603 the general metabolism[53,54]. The Hap complex is the major regulator of this shift, controlling
604 respiration and mitochondrial function in this yeast[55,56]. In pathogenic fungi, this complex has been
605 studied mostly for its ambivalent regulatory function in iron metabolism[57–59]. As in *S. cerevisiae* [60], the
606 Hap complex seems to control respiration in *C. neoformans*. Thus, Hap3 and HapX have also been
607 shown to negatively regulate genes encoding respiratory and TCA cycle function under low iron
608 condition[61]. We observed an increase in the mitochondria number in the *gat5Δ* background and to a
609 lesser extent in *hap2Δ* one. The *HAP* genes have also been shown to regulate sexual development in
610 association with the pheromone-responsive Cpk1 mitogen-activated protein kinase pathway in this
611 pathogenic yeast[40]. However, phenotypic analyses of the *hap* mutants suggest that HapX and the
612 Hap2/3/5 complex might also have independent functions. For instance, *HAP3* and *HAP5* but not *HAPX*
613 are necessary for growth on ethanol[59], and the Hap2/3/5 complex, but not HapX, is crucial in
614 repressing pheromone production and cell fusion during mating[40]. Similarly, we found that the
615 Hap2/3/5 complex, but not HapX, controls FLC resistance and EV production in *C. neoformans*.
616 The FLC resistance phenotype of the *hap* mutant strains is consistent with the literature[61,62].
617 Counterintuitively, Hap3 and HapX have been reported to positively regulate several ergosterol
618 biosynthetic genes[61]. Our differential gene expression analysis, which used different growth
619 conditions, identified only two genes, *ERG20* (CNAG_02084) and *ERG27* (CNAG_07437)
620 downregulated and one upregulated, *IDI1* (CNAG_00265) upon *HAP2* deletion. Overall, these data
621 suggest that Hap2 in *C. neoformans* regulates global cellular changes impacting fluconazole resistance
622 beyond the regulation of the ergosterol pathway.
623 In this work, we present cumulative lines of evidence suggesting a causative link between FLC
624 resistance and EV production. First, all four EV production mutants displayed altered FLC susceptibility.

625 We also observed this association with other hap mutants; *hapxΔ* being the only one producing WT
626 level of EVs yet diplaying a slight change in FLC suceptibilty. Second, all spontaneous FLC-resistant
627 mutant strains isolated *in vitro* reduced the EV production, and both phenotypes reverted jointly.
628 Because most of these spontaneous FLC mutant strains are also aneuploid and often disomic for
629 chromosome 1 (known to bear *ERG11* and *AFR1*[12]), one can imagine that a gene repressing EV
630 production could also be located on chromosome 1. In that case, disomy of this chromosome would
631 result in both the increased expression of FLC-resistant genes and EV repressors. Although possible,
632 this hypothesis is not the only one. We also identified two FLC-resistant spontaneous mutant strains
633 with no duplication of chromosome 1; one being disomic of chromosome 4 and one presenting a
634 higher number of mitochondria per cell. Interestingly, none of the EV production regulators identified
635 here are located on chromosome 1. Finally, although we did not observe any correlations between
636 the level of drug resistance and EV production among clinical isolates, the analysis of a couple of serial
637 isolates from the same patient for which no mutation classically involved in FLC resistance could be
638 identified revealed that the resistant strain produced lower EV amounts compared to the sensitive
639 one. Notably, we did not observe any changes in chromosome copy numbers in these strains.
640 Moreover, a sensitive strain derived from a resistant clinical isolate obtained after several passages in
641 a drug-free medium produces more EVs than the original strain. This reinforces the idea that EV
642 production and FLC resistance are strongly linked, at least in a subset of genetic backgrounds.

643 Nevertheless, the mechanism by which Hap2 and Gat5 regulates both EV production and FLC
644 susceptibility remains unknown. We observed overexpression of the drug efflux pumps *AFR1* and *AFR3*
645 in *gat5Δ,* which could contribute to the resistance phenotype. We also observed an alteration of
646 lanosterol/ergosterol equilibrium in the presence of FLC in the EV-deficient mutants, which could
647 explain a modification of drug resistance. Indeed, a recent report revealed that targeting plasma
648 homeostasis using drugs is enough to modify azole resistance in pathogenic fungi[63]. However, it is
649 unclear whether the decreased EV production alters plasma membrane homeostasis or whether these
650 two TFs regulate plasma membrane homeostasis and, consequently, EV production. Previous data in
651 *Cryptococcus* suggest that the deletion of genes implicated in plasma membrane homeostasis can
652 impact EV production and/or cargo loading[64,65]**.** On the other hand, the fact that most EV structural
653 protein-encoding genes are strongly downregulated in both *gat5Δ* and *hap2Δ* mutant strains suggests
654 a direct effect of these TF on EV biosynthesis. The fact that a Y145F *ERG11* mutation regulates FLC
655 resistance without altering EV production also favors this second hypothesis.

656 Interestingly, we found that a low concentration of FLC reduces EV production. Yet, this
657 concentration is not sufficient to alter the *ERG11* gene expression, suggesting that cells might regulate
658 EV production to maintain plasma membrane homeostasis. The impact of low concentration of

antifungal on fungal cell biology and drug resistance acquisition in pathogenic fungi is poorly studied [6,66], but our data clearly shows that fungal cells can regulate EV production before regulating gene expression, which might suggest a first line of defense under membrane stress. In this model (**Fig 14**), different mutations or FLC concentrations trigger three types of cellular responses; *ERG11* overexpression and EV production would regulate plasma membrane ergosterol content or more broadly membrane homeostasis, whereas regulation of efflux pump would alter FLC concentrations in the cell.

Overall, this study identified the first TF regulating fungal EV biosynthetic pathways, but it also raised new questions in this field of research. The genetics of EV production is still in its infancy, but functional genetics will further our understanding of EV biogenesis, their impact on drug resistance, and their roles during fungal infection.

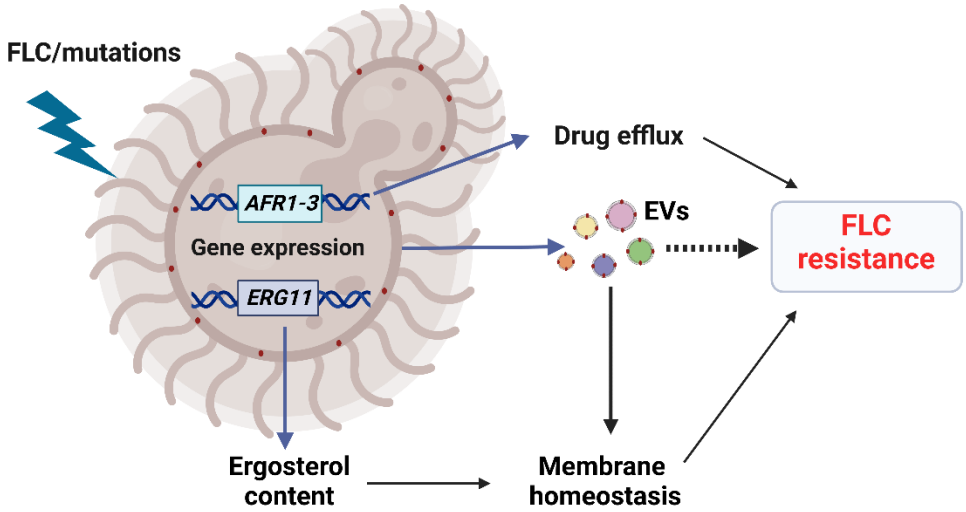


**Figure 14:** Model of EV biogenesis regulation and FLC susceptibility in *C. neoformans*. Specific gene mutations (such for the transcription factors *HAP2* and *GAT5*) and cell exposure to fluconazole (FLC) can trigger diverse types of cellular responses: changes in the expression of drug efflux-associated genes (*AFR1-3*), in the expression of the azole target gene *ERG11*, or ~~in~~ EV biogenesis. The regulation of efflux pump expression would alter intracellular FLC concentration, whereas both *ERG11* overexpression~~,~~ and regulation of EV biogenesis would alter fungal plasma membrane lipid homeostasis. The differential regulation of these cellular processes might determine FLC resistance phenotypes in this fungal pathogen. Schematic model created in BioRender.

## 5) Acknowledgments

JR was supported by the Pasteur-Roux-Cantarini fellowship of Institut Pasteur and by FAPERJ - Fundação de Amparo à Pesquisa do Estado do Rio de Janeiro (E-26/204.456/2021). This work was supported by a CAPES COFECUB grant n°39712ZK to GJ, MLR, and LN. The work was supported by an ANR grant (Projet ResistEV AAPG2021 CE35) to GJ, IVE and AA, T.T.V.D was supported by the Pasteur -

685 Paris University (PPU) International PhD Program. IVE is supported by a CIFAR Azrieli Global Scholar
686 Award. We would like to thank in particular Laëtitia Viengsavanh for the help with the initial steps of
687 TF mutant collection screening, and some members of the French Cryptococcosis Study Group:
688 Christine Bonnal (Hôpital Bichat-Claude Bernardn Paris), Marie-Elisabeth Bougnoux (Hôpital Necker-
689 Enfants Malades, Paris), Nathalie Bourgeois (CHU Montpellier), Sophie Cassaing (CHU Toulouse), Lilia
690 Hasseine (CHU Nice), and Stéphane Ranque (IHU Méditerranée Infection, Marseille).
691

692 **6) Author contributions**

693 J.R., A.T., and F.M. performed the transcription factor mutant library screening for EV production, drug
694 susceptibility assays, isolation of *in vitro* clinical isolates, growth passages and RT-qPCR analyses. F.M.
695 and I.M. helped with the mutant construction. J.Y.C. and JR prepared the DNA and RNA sequencing
696 libraries. C.M. performed the sequencing library trimming, mapping and bioinformatic analyses. P.C.
697 and S.N. helped with the nanoflow cytometry analyses. I.V.E. advised on drug susceptibility assays and
698 experimental design. G.P.A. performed cryo-electron microscopy analyses. L.N. and A.G.Z. performed
699 the lipid analysis. T.T.V.D. and J.R. performed the gene complementations. A.A and M.D. selected the
700 clinical strains to be studied. J.R. and G.J. conceived and designed the project. G.J. and M.L.R.
701 supervised the research. J.R. and G.J. wrote the manuscript. All authors commented on the final
702 version. All authors have read and agreed to the published version of the manuscript.
703

704 **7) References**

705

706 1. Fisher, M. C. *et al.* Threats Posed by the Fungal Kingdom to Humans, Wildlife, and Agriculture.
707 *mBio* **11**, e00449-20 (2020).
708 2. Janbon, G., Quintin, J., Lanternier, F. & d'Enfert, C. Studying fungal pathogens of humans and
709 fungal infections: fungal diversity and diversity of approaches. *Genes Immun* **20**, 403–414 (2019).
710 3. Brown, G. D. *et al.* Hidden killers: human fungal infections. *Science translational medicine* **4**,
711 165rv13 (2012).
712 4. WHO fungal priority pathogens list to guide research, development and public health action.
713 https://www.who.int/publications-detail-redirect/9789240060241.
714 5. Rajasingham, R. *et al.* Global burden of disease of HIV-associated cryptococcal meningitis: an
715 updated analysis. *The Lancet Infectious Diseases* **17**, 873–881 (2017).

716 6. Fisher, M. C. *et al.* Tackling the emerging threat of antifungal resistance to human health. *Nat Rev*
717 *Microbiol* **20**, 557–571 (2022).
718 7. Almeida, F., Rodrigues, M. L. & Coelho, C. The Still Underestimated Problem of Fungal Diseases
719 Worldwide. *Frontiers in Microbiology* **10**, (2019).
720 8. Robbins, N., Caplan, T. & Cowen, L. E. Molecular Evolution of Antifungal Drug Resistance. *Annu*
721 *Rev Microbiol* **71**, 753–775 (2017).
722 9. Berman, J. & Krysan, D. J. Drug resistance and tolerance in fungi. *Nat Rev Microbiol* **18**, 319–331
723 (2020).
724 10. Rodero, L. *et al.* G484S Amino Acid Substitution in Lanosterol 14-α Demethylase (ERG11) Is
725 Related to Fluconazole Resistance in a Recurrent Cryptococcus neoformans Clinical Isolate.
726 *Antimicrobial Agents and Chemotherapy* **47**, 3653–3656 (2003).
727 11. Sionov, E., Lee, H., Chang, Y. C. & Kwon-Chung, K. J. Cryptococcus neoformans Overcomes
728 Stress of Azole Drugs by Formation of Disomy in Specific Multiple Chromosomes. *PLOS Pathogens*
729 **6**, e1000848 (2010).
730 12. Stone, N. R. H. *et al.* Dynamic ploidy changes drive fluconazole resistance in human
731 cryptococcal meningitis. *Journal of Clinical Investigation* **129**, 999–1014 (2019).
732 13. Rizzo, J., Rodrigues, M. L. & Janbon, G. Extracellular Vesicles in Fungi: Past, Present, and
733 Future Perspectives. *Front. Cell. Infect. Microbiol.* **10**, 346 (2020).
734 14. Rizzo, J. *et al. Cryptococcus* extracellular vesicles properties and their use as vaccine
735 platforms. *Journal of Extracellular Vesicles* **10**, (2021).
736 15. Zhao, M. *et al.* Turbinmicin inhibits Candida biofilm growth by disrupting fungal vesicle–
737 mediated trafficking. *Journal of Clinical Investigation* **131**, e145123 (2021).
738 16. Demuyser, L., Van Dyck, K., Timmermans, B. & Van Dijck, P. Inhibition of Vesicular Transport
739 Influences Fungal Susceptibility to Fluconazole. *Antimicrob Agents Chemother* **63**, e01998-18
740 (2019).

741 17. Estrada, A. F., Muruganandam, G., Prescianotto-Baschong, C. & Spang, A. The ArfGAP2/3
742 Glo3 and ergosterol collaborate in transport of a subset of cargoes. *Biol Open* **4**, 792–802 (2015).
743 18. Walton, F. J., Heitman, J. & Idnurm, A. Conserved elements of the RAM signaling pathway
744 establish cell polarity in the basidiomycete Cryptococcus neoformans in a divergent fashion from
745 other fungi. *Mol Biol Cell* **17**, 3768–3780 (2006).
746 19. Wambaugh, M. A. *et al.* Synergistic and antagonistic drug interactions in the treatment of
747 systemic fungal infections. *Elife* **9**, e54160 (2020).
748 20. Zarnowski, R. *et al.* Candida albicans biofilm-induced vesicles confer drug resistance through
749 matrix biogenesis. *PLoS Biol* **16**, e2006872 (2018).
750 21. Chan, W. *et al.* Induction of amphotericin B resistance in susceptible *Candida auris* by
751 extracellular vesicles. *Emerging Microbes & Infections* **11**, 1900–1909 (2022).
752 22. Zarnowski, R. *et al.* Coordination of fungal biofilm development by extracellular vesicle
753 cargo. *Nat Commun* **12**, 6235 (2021).
754 23. Zhao, K. *et al.* Extracellular vesicles secreted by Saccharomyces cerevisiae are involved in cell
755 wall remodelling. *Commun Biol* **2**, 1–13 (2019).
756 24. Douanne, N. *et al.* Leishmania parasites exchange drug-resistance genes through
757 extracellular vesicles. *Cell Reports* **40**, 111121 (2022).
758 25. Jung, K.-W. *et al.* Systematic functional profiling of transcription factor networks in
759 Cryptococcus neoformans. *Nat Commun* **6**, 6757 (2015).
760 26. Cui, W., Li, X., Hull, L. & Xiao, M. GATA-type transcription factors play a vital role in radiation
761 sensitivity of Cryptococcus neoformans by regulating the gene expression of specific amino acid
762 permeases. *Sci Rep* **9**, 6385 (2019).
763 27. Yi, J. *et al.* Transcription factor Liv4 is required for growth and pathogenesis of *Cryptococcus*
764 *neoformans*. *FEMS Yeast Research* **20**, foaa015 (2020).
765 28. Mao, Y. & Chen, C. The Hap Complex in Yeasts: Structure, Assembly Mode, and Gene
766 Regulation. *Front. Microbiol.* **10**, 1645 (2019).

767 29. Fuge, E. K., Braun, E. L. & Werner-Washburne, M. Protein synthesis in long-term stationary-
768 phase cultures of Saccharomyces cerevisiae. *J Bacteriol* **176**, 5802–5813 (1994).
769 30. Gow, N. A. R. *et al.* The importance of antimicrobial resistance in medical mycology. *Nat*
770 *Commun* **13**, 5352 (2022).
771 31. Jordá, T. & Puig, S. Regulation of Ergosterol Biosynthesis in Saccharomyces cerevisiae. *Genes*
772 *(Basel)* **11**, 795 (2020).
773 32. Foresti, O., Ruggiano, A., Hannibal-Bach, H. K., Ejsing, C. S. & Carvalho, P. Sterol homeostasis
774 requires regulated degradation of squalene monooxygenase by the ubiquitin ligase Doa10/Teb4.
775 *Elife* **2**, e00953 (2013).
776 33. Mondon, P. *et al.* Heteroresistance to fluconazole and voriconazole in Cryptococcus
777 neoformans. *Antimicrob Agents Chemother* **43**, 1856–1861 (1999).
778 34. Sionov, E. *et al.* Identification of a Cryptococcus neoformans Cytochrome P450 Lanosterol
779 14α-Demethylase (Erg11) Residue Critical for Differential Susceptibility between
780 Fluconazole/Voriconazole and Itraconazole/Posaconazole | Antimicrobial Agents and
781 Chemotherapy. https://journals.asm.org/doi/10.1128/AAC.05502-11.
782 35. Janbon, G., Himmelreich, U., Moyrand, F., Improvisi, L. & Dromer, F. Cas1p is a membrane
783 protein necessary for the O-acetylation of the Cryptococcus neoformans capsular polysaccharide.
784 *Molecular Microbiology* **42**, 453–467 (2001).
785 36. Janbon, G. *et al.* Analysis of the Genome and Transcriptome of Cryptococcus neoformans
786 var. grubii Reveals Complex RNA Expression and Microevolution Leading to Virulence
787 Attenuation. *PLoS Genet* **10**, e1004261 (2014).
788 37. Nielsen, K. *et al.* Sexual cycle of Cryptococcus neoformans var. grubii and virulence of
789 congenic a and alpha isolates. *Infect Immun* **71**, 4831–4841 (2003).
790 38. Lin, J., Fan, Y. & Lin, X. Transformation of Cryptococcus neoformans by electroporation using
791 a transient CRISPR-Cas9 expression (TRACE) system. *Fungal Genet Biol* **138**, 103364 (2020).

792 39. Arras, S. D. M., Chitty, J. L., Blake, K. L., Schulz, B. L. & Fraser, J. A. A Genomic Safe Haven for
793 Mutant Complementation in Cryptococcus neoformans. *PLOS ONE* **10**, e0122916 (2015).
794 40. Tian, Y. *et al.* Quality and efficiency assessment of six extracellular vesicle isolation methods
795 by nano-flow cytometry. *Journal of Extracellular Vesicles* **9**, 1697028 (2020).
796 41. Moyrand, F., Lafontaine, I., Fontaine, T. & Janbon, G. UGE1 and UGE2 regulate the UDP-
797 glucose/UDP-galactose equilibrium in Cryptococcus neoformans. *Eukaryot Cell* **7**, 2069–2077
798 (2008).
799 42. Medical Mycology: Cellular and Molecular Techniques | Wiley. *Wiley.com*
800 https://www.wiley.com/en-us/Medical+Mycology%3A+Cellular+and+Molecular+Techniques-p-
801 9780470057407.
802 43. Wallace, E. W. J. *et al.* Quantitative global studies reveal differential translational control by
803 start codon context across the fungal kingdom. *Nucleic Acids Res* **48**, 2312–2331 (2020).
804 44. Langmead, B. & Salzberg, S. L. Fast gapped-read alignment with Bowtie 2. *Nat Methods* **9**,
805 357–359 (2012).
806 45. Kim, D. *et al.* TopHat2: accurate alignment of transcriptomes in the presence of insertions,
807 deletions and gene fusions. *Genome Biol* **14**, R36 (2013).
808 46. Love, M. I., Huber, W. & Anders, S. Moderated estimation of fold change and dispersion for
809 RNA-seq data with DESeq2. *Genome Biol* **15**, 550 (2014).
810 47. Maufrais, C. *et al.* Population genomic analysis of Cryptococcus Brazilian isolates reveals an
811 African type subclade distribution. *G3 (Bethesda)* **11**, jkab107 (2021).
812 48. Li, H. Minimap2: pairwise alignment for nucleotide sequences. *Bioinformatics* **34**, 3094–3100
813 (2018).
814 49. Li, H. *et al.* The Sequence Alignment/Map format and SAMtools. *Bioinformatics* **25**, 2078–
815 2079 (2009).
816 50. Rosenberg, A. *et al.* Antifungal tolerance is a subpopulation effect distinct from resistance
817 and is associated with persistent candidemia. *Nat Commun* **9**, 2470 (2018).

818 51. Cleare, L. G. *et al.* Media Matters! Alterations in the loading and release of Histoplasma
819 capsulatum extracellular vesicles in response to different nutritional milieus. *Cellular*
820 *Microbiology* **n/a**, e13217.
821 52. Reis, F. C. G. *et al.* Analysis of Cryptococcal Extracellular Vesicles: Experimental Approaches
822 for Studying Their Diversity Among Multiple Isolates, Kinetics of Production, Methods of
823 Separation, and Detection in Cultures of Titan Cells. *Microbiol Spectr* **9**, e0012521 (2021).
824 53. Werner-Washburne, M., Braun, E., Johnston, G. C. & Singer, R. A. Stationary phase in the
825 yeast Saccharomyces cerevisiae. *Microbiol Rev* **57**, 383–401 (1993).
826 54. Galdieri, L., Mehrotra, S., Yu, S. & Vancura, A. Transcriptional regulation in yeast during
827 diauxic shift and stationary phase. *OMICS* **14**, 629–638 (2010).
828 55. S, B. *et al.* The S. Cerevisiae HAP complex, a key regulator of mitochondrial function,
829 coordinates nuclear and mitochondrial gene expression. *Comparative and functional genomics* **4**,
830 (2003).
831 56. Bolotin-Fukuhara, M. Thirty years of the HAP2/3/4/5 complex. *Biochim Biophys Acta Gene*
832 *Regul Mech* **1860**, 543–559 (2017).
833 57. Singh, R. P., Prasad, H. K., Sinha, I., Agarwal, N. & Natarajan, K. Cap2-HAP complex is a critical
834 transcriptional regulator that has dual but contrasting roles in regulation of iron homeostasis in
835 Candida albicans. *J Biol Chem* **286**, 25154–25170 (2011).
836 58. Gsaller, F. *et al.* The Janus transcription factor HapX controls fungal adaptation to both iron
837 starvation and iron excess. *EMBO J* **33**, 2261–2276 (2014).
838 59. Jung, W. H. *et al.* HapX positively and negatively regulates the transcriptional response to
839 iron deprivation in Cryptococcus neoformans. *PLoS Pathog* **6**, e1001209 (2010).
840 60. Buschlen, S. *et al.* The S. Cerevisiae HAP complex, a key regulator of mitochondrial function,
841 coordinates nuclear and mitochondrial gene expression. *Comp Funct Genomics* **4**, 37–46 (2003).
842 61. Kim, J. *et al.* A defect in iron uptake enhances the susceptibility of Cryptococcus neoformans
843 to azole antifungal drugs. *Fungal Genet Biol* **49**, 955–966 (2012).

844 62. Caza, M., Hu, G., Price, M., Perfect, J. R. & Kronstad, J. W. The Zinc Finger Protein Mig1
845 Regulates Mitochondrial Function and Azole Drug Susceptibility in the Pathogenic Fungus
846 Cryptococcus neoformans. *mSphere* **1**, e00080-15 (2016).
847 63. Revie, N. M. *et al.* Targeting fungal membrane homeostasis with imidazopyrazoindoles
848 impairs azole resistance and biofilm formation. *Nat Commun* **13**, 3634 (2022).
849 64. Reis, F. C. G. *et al.* A Novel Protocol for the Isolation of Fungal Extracellular Vesicles Reveals
850 the Participation of a Putative Scramblase in Polysaccharide Export and Capsule Construction in
851 Cryptococcus gattii. *mSphere* **4**, (2019).
852 65. Rizzo, J. *et al.* Role of the Apt1 protein in polysaccharide secretion by Cryptococcus
853 neoformans. *Eukaryotic cell* **13**, 715–26 (2014).
854 66. Handelman, M. & Osherov, N. Experimental and in-host evolution of triazole resistance in
855 human pathogenic fungi. *Frontiers in Fungal Biology* **3**, (2022).
856
857
858
859
860
861
862
863